

MEM-493: Senior Design

Spring Term Report

PR 33: Design of an Automated Couette Viscometer

Date: 13 May 2015

Advisor: Professor Young Cho

Group Members:

Austin Farber

Rich Hanna

Matthew Lorenz

Dan Nguyen

Michael Sinisi



Table of Contents

Abstract	4
Introduction	4
Problem Statement.....	4
Needs & Specifications.....	4
Theory	5
Methods	5
Embodiment & Prototyping	7
<i>Rotor Development</i>	7
<i>Temperature Control</i>	7
<i>Housing Development</i>	8
Detail Design	8
<i>Rotor</i>	8
<i>Motor</i>	9
<i>Magnetic Field</i>	9
<i>Temperature Control</i>	9
<i>Housing</i>	10
Discussion	10
Verification.....	10
<i>Incorporated Standards</i>	10
<i>Viscosity</i>	10
<i>Hemolysis</i>	11
<i>Thermal Retention</i>	11
<i>Dimension Analysis</i>	12
<i>Magnetic Field</i>	12
<i>Dynamic Eccentricity</i>	12
<i>Eddy Current</i>	12
Limitations.....	12
<i>Rotor</i>	12
<i>Vibration</i>	13
Context & Impact	13
Economic Analysis	13
Environmental Impact Analysis.....	14
Social Impact Analysis	14
Ethical Analysis.....	14
Project Management	14
Team Organization.....	14
Schedule and Milestones	15

Project Budget.....	15
Summary & Conclusions	15
Future Work.....	16
References.....	17
Appendix A: Needs & Specifications.....	18
Appendix B: Detailed Theory	20
<i>Viscosity</i>	20
<i>Couette Flow</i>	20
<i>Viscometry</i>	21
<i>Eddy Current</i>	21
<i>Buoyancy</i>	22
<i>Heat Transfer</i>	23
<i>Measuring Viscosity Experimentally</i>	23
Appendix C: Final Assembly & Device Renders.....	26
Appendix D: Final Electrical Diagram & Programming Schematic	28
Appendix E: Rotor Development & Prototyping	29
Appendix F: Thermal Control Development & Prototyping.....	33
Appendix G: Housing Development & Prototyping.....	34
Appendix H: Experimental Results.....	36
Appendix I: Experimental and Developmental Protocols.....	44
Appendix J: Bill of Materials.....	50
Appendix K: Final Gantt Chart	50

Abstract

Blood viscosity can be correlated with cardiovascular disease (CVD) and other microvascular disorders. In the field of preventative medicine, such a metric can help monitor patient health and detect cardiovascular risk factors. We propose a Couette flow viscometer specifically designed to accommodate non-Newtonian fluids such as blood. Rotation of the inner of two coaxial cylinders, induced via eddy current, is used to measure the torque applied to the shear stress of a fluid trapped between the two cylinders. By control of a DC motor, a rotating magnetic field will induce the rotation and allow for data collection over a range of low shear rates. This device assists physicians and researchers alike with the option to output specific values or full viscosity profiles. It also enriches the quantitative blood viscosity data that is currently available, thus improving the potential to predict the onset of CVD.

Introduction

Problem Statement

The mission of this project is to develop a device capable of analyzing blood viscosity over a range of speeds by control of an automated Couette flow viscometer with the ability to dispose of elements coming in contact with the fluid sample. The project looks to offer a new tool to the fields of diagnostic and preventative medicine; a platform that may help patients and physicians to improve wellness and contribute to health monitoring.

Measuring the viscosity of blood is becoming extremely important in the field of cardiovascular diseases with experts claiming that the viscosity of a person's blood directly affects their health^[1]. Highly viscous blood is more difficult for the heart to pump throughout the body and heightens a patient's risk of clotting within their vasculature. The combination of a heart under greater stress and a higher probability of vascular thrombogenesis is associated with various cardiovascular health risks including high blood pressure, type II diabetes, and obesity. Additionally, low viscosity blood can lead to renal malfunction or extremely low blood glucose and cholesterol levels^[2]. These are the result of a low viscosity fluid's turbulent flow. For these reasons, medical professionals would find it beneficial to monitor a patient's blood viscosity. By monitoring this metric, prescription drugs, such as blood thinners and thickeners, and other preventative measures can be applied to ensure a healthy heart.

There are three main issues concerning blood viscosity measurement:

1. Sample volume must be minimized for measurement accuracy and patient compliance.
2. Viscosity cannot be defined by the linear relationship between shear rate and fluid motion because blood is a non-Newtonian fluid.
3. Measurement is sanitary, cost and time sensitive.

Needs & Specifications

This project has identified a number of potential populations that would have specific interests in the development of an automated blood viscometer. The medical community (i.e. doctors, physicians, hospitals and clinics) would benefit from having a medical device that could help to better serve their patients. Although not a relatively new technology, the innovations and improvements proposed in this viscometer would be markedly advantageous to anyone who uses, or has considered using, such a device. The device has the potential to directly impact patient wellness and determine the presence of hematological cardiovascular risk factors. University personnel and scientific specialists will find that this device may help with making advances in their fields of research. Any studies regarding the viscosity of a non-Newtonian fluid would benefit from a more efficient version of current market technologies.

Appendix A contains a full list of needs and specifications, along with a priority ranking for each one. The key driving specifications are: the addition of a rheostat motor with a control system capable of slowing sample rotation to 0 RPM in approximately 1 minute and the requirement that the device shall produce a range of rotational speeds ($F_s < 600\text{Pa}^{[3]}$). The success of this project relies on the ability of the senior design group to fulfill these two specifications while addressing all remaining needs. A failure to meet either of these will ultimately lead to the production of a device that is incapable of meeting stakeholder needs.

Theory

The automated Couette viscometer relies heavily on theory ranging from a breadth of concepts and principles. In the interest of being succinct, detailed explanations of each theoretical concept can be found in Appendix B of this report, but a brief discussion of their use are given below.

First and foremost, an understanding of *Viscosity* and its physical applications must be understood in order to properly analyze and calculate it over a range of environmental behaviors and a range of different fluidic subjects. *Couette Flow*, the driving force behind this project, involves three main components: a stationary outer cylinder, a rotational inner cylinder, and the fluid to be analyzed trapped in between. Viscosity can be obtained by analyzing the rotational speed of the inner cylinder due to material properties of the test fluid and shear stresses imposed upon it. To control Couette flow without tangibly interacting with the inner cylinder, use of *Eddy Current* principles through rotating magnets induce the flux needed to drive the desired rotation. To further ensure that no tangible interaction is necessary with the inner cylinder, *Buoyancy* plays a key factor in avoiding any frictional contact between the coaxial cylinders. Any friction would nullify viscosity measurements and void any analysis. Since this project relies on simulation of the internal human environment, maintaining proper temperature akin to human body temperature (36.9°C) is crucial for proper blood sample analysis.

Methods

The development and design of the automated Couette viscometer took on a significant number of changes in comparison to the original breakdown followed in the fall term and updated design in the winter term. As roles held by team members took on overlapping responsibilities and the project itself transformed from a virtual nature to a physical one, redefinition of the device became necessary.

As discussed in previous terms, the success of the device depends upon completion and accuracy of a number of core areas that are laid out in detail device dissection (Figure C-2). Samples are placed within the Coaxial Fluid Tester, which is comprised of a ferrous yet buoyant rotor, a vacutainer, and the test fluid for which viscosity values are to be determined. All components of the Coaxial Fluid Tester are disposable for sanitation purposes. Aluminum was designated the material of choice for the rotor to maximize application of eddy current induced rotation; however, experimentation of a unibody aluminum rotor yielded that using solely metal would compromise the necessary buoyancy required. Therefore a hybrid PPR-aluminum rotor was designed. This rotor maximizes buoyancy force in order to counteract gravitational force and thereby nullify any friction caused between the rotor and the vacutainer that could skew viscosity readings.

Rotation via eddy current is facilitated and controlled by strategic placement of bar magnets within a PVC tube fixture. The bar magnets have been fixed in a vertical position, as opposed to the original horizontal one, to increase magnetic field strength. After completed testing in the winter term, it was deemed that four neodymium magnets, spaced contralateral from one another and approximately 1" apart, were necessary for proper rotation. This fixture is connected to a screw hub and motor that comprises the Rotational Assembly of the device. The Rotational Assembly is controlled via programming logic and electrical components as supplied by the Rotalink software package. To ensure proper stability and the aesthetic enclosure of these components, the Housing is made to define the base, foundation and address any shock absorption concerns generated by rotation. A drawing of the current motor base can be seen in Figure G-2. A rendering of the full prototype setup is shown in Figure C-1.

As mentioned previously, it is immensely important that the device be capable of keeping fluid samples, such as blood, at temperatures akin to human body temperature (36.9°C). Originally a heat pump was to be used to maintain this requirement but it was found to be too spatially taxing and expensive. After the winter term, a glass enclosure for the Coaxial Fluid Tester was to be used containing eicosane was for thermal retention. However, with the updated proximity of the magnets to the ferrous rotor, sizing constraints made this idea impossible to implement. Instead, samples of blood will be kept at human body temperature in an exterior heated casing. This casing is made of a combination of aluminum and wood with pores that can hold each vacutainer for a total of five samples. Heating strips maintain the desired temperature until the samples are ready to be tested and placed into the Rotational Assembly.

This viscometer is comprised of three electrical aspects. Powering the system was crucial, but this made motor control and data acquisition possible. The schematic showing all hardware can be seen in Figure D-1. Programming logic is attributed to the Rotalink hardware as shown in the sample schematic in Figure D-2. However, as opposed to previous terms where "coasting" behavior was desired, it was found that once the Rotational Assembly's motion ceased, the rotation of the inner rotor also stopped. The programming now automatically assigns changing speeds in steps to bring the rotational speed of the rotor down in increments while retaining the ability to observe viscous behavior over varying speeds. By its implementation, motor revolutions per minute can be controlled at varying automated speeds to achieve the goal of reading viscosity behavior over low shear rates. In order to acquire readable data, the rotor from the Coaxial Fluid Tester is affixed with a strip of reflective tape at a height on level with the tachometer. Every rotation of the reflective tape denotes a reading on the tachometer and allows for the calculation of rotational speed; speed curves for different fluids with known viscosities are compared to the curve for blood to determine its viscosity. The motor used to power the Rotational Assembly requires 12V direct current (DC), as seen in Figure D-1. However, because the priority stakeholders require power to be supplied from an outlet with alternating current (AC), an AC/DC converter is used to take the outlet 120V AC at 60 Hz and convert it to 12V DC. The tachometer also runs on 12V DC.

Design Description

Embodiment & Prototyping

Rotor Development

Fabrication

Initially cylindrical constructs were lathed from a solid 7075 aluminum rod to the geometry, shown in Appendix E, based on the theoretical buoyancy calculations. Rotors were created for both 10mL and 4.5mL sizes. The volume of each rotor was minimized to achieve a buoyancy force greater than the rotor weight; however, manufacturing constraints limited the extent to which the rotor walls could be thinned. Unfortunately this rotor was still too heavy to float in such a small fluid volume.

In lieu of a unibody rotor, made entirely of a single material, a hybrid material design was found to overcome these limitations. In summary, a polymer serves as the outer body of the rotor and an aluminum tube placed inside is the rotational driver. This method ensures enough surface area to generate rotation via eddy current as well as a minimized rotor weight. Notches along the inner lumen of the polymer component mechanically join the two materials so that rotation of the aluminum is transferred to the outer body without needing to adhere them together. The rotational driver is a slightly less dense 6061 Aluminum prefabricated tube while the photopolymer resin (PPR) is rapid prototyped via stereolithography (SLA). This additive fabrication technique was selected due to its high precision and selection of material properties. The final rotor design is shown in Appendix E.

Temperature Control

Fabrication

The body of the Temperature Control system was designed to encase the thermal cord between two aluminum blocks in order to promote thermal conductivity. Annotated drawings of these blocks can be seen in Figures F-1 and F-2. The aluminum was purchased from McMaster Carr and milled down to size in the Drexel machine shop. Each block was then milled down the center of one face, so when the blocks are pressed against one another they create a gap just large enough for the heating element. The manual mill was then used to drill the five holes for vacutainers in the top block, which required first drilling out $\frac{1}{2}$ " deep holes in the correct positions, then drilling 2.5" deep pilot holes for the larger drill bit ($\frac{1}{2}$ " diameter) to come through. The mill was finally used to drill small holes in both the top and bottom block in order to create a space for pegs to lock the two components together. The pegs were made from $\frac{1}{4}$ " round stock, first cut to approximate size on the bandsaw and then faced to exact dimensions on a manual lathe. The pegs were inserted into the holes on the bottom block of aluminum, and the top block matched them adequately. Once this structure was complete, a small wooden housing was laser-cut to shape and placed around the aluminum in order to insulate the system.

These manufactured components interface with the purchased components adequately, as the milled aluminum groove fits the heating cord, and the power cable is long enough to reach around the aluminum housing to the purchased control box. The control box is set to heat the samples to approximately 98-100°F (36.67-37.78°C), which causes the heating element at the base of the manufactured aluminum to increase in temperature until the thermocouple at the top of the aluminum detects it is in that range.

Material

Aluminum was chosen for the inside of the thermal housing as it is a highly thermally conductive material and it is easy to machine. Previous iterations of the thermal system did not allow aluminum as it would interfere with eddy current rotation, but now that the heating system is separate from the Rotational Assembly, aluminum is acceptable and even preferred.

Craft plywood was chosen to insulate the aluminum because it is easy to fabricate with, it is cost effective, and it has a low thermal conductivity (plywood, $k = 0.13$ | aluminum, $k = 205$). After creating the majority of the enclosure on the laser cutter, it was a very quick and simple process to create a new design file for the heating enclosure and execute it on the laser cutter.

Housing Development

Fabrication

First the CAD model of the two-drum design was dimensionally updated in order to determine the arc length of each of the drums. The footprint of the walls was then offset by half the wall thickness (1.5mm) and the two arc lengths were dimensionally updated. These lengths were used to determine the length of material required for each curve of the housing walls, and an Adobe Illustrator file was generated for laser cutting. The laser cutter scored a series of vertical lines in two sheets of 3mm medium-density fiberboard (MDF) in order to increase their flexibility, so they were able to wrap around the MDF base. The base and roof were laser cut from 3mm MDF as well, in order to be consistent in terms of look, weight, and feel between enclosure materials. The dimensions of the base were determined from the arc measurements taken before the wall offset calculation, so the walls would be able to fit around the base instead of being placed directly on it. This allowed for better contact between the walls and the base while they were adhered together with wood glue, resulting in a sturdy structure matching the original plans. The roof measurements took into account the wall offset, so the rounded roof platforms were made slightly larger than the base platform. These components include an added MDF lip glued to the underside, allowing them to lock onto the walls and easily remove as well. The completed housing can be seen in Figure G-3.

Material

MDF was chosen as the main enclosure material primarily due to the flexible fabrication technique seen in the final design. There are only a few manufacturing techniques available in order to fabricate the curved walls of the housing. It would actually be easier to purchase an aluminum sheet and use a roller to shape the drums, but wrapping the eddy current system in a conductive material would only lead to rotational problems, so it was important to create the housing out of something other than metal. Scoring MDF with a laser in order to create a flexible joint or a “living hinge” is common amongst laser hobbyists, so a matter of applying such methods yielded the ideal final result.

Detail Design

Rotor

Replacing the outer portion of the rotor with photopolymer resin (PPR) is possible based on its material properties. PPR is capable of being heated to 36.9°C without significant deformation due to a glass transition temperature of 53°C and an appropriate density only 10.3% higher than blood at approximately 0.0426 lb/in³ [14]. However, in addition to its slight porosity, the current PPR material is not FDA compliant as biocompatible^[14]. Thus, for future production of this component, other materials and additive manufacturing methods should be considered. For additional details about the rotor, refer to Appendix E.

Motor

The purpose of the motor is to induce rotation of the rotor mechanism. The rotation of the rotor is dependent on the creation of eddy current. During the fall term, there was a specification that the motor would have to spin at 50 RPM, but after much testing and research^[13], it has been determined that much higher rotational speeds are necessary to cause the rotation through eddy current. For this reason, the team purchased a stronger motor from Rotalink, which has a maximum speed of 9000 RPM at 12V DC with an 8:1 gear ratio. This combination allows the motor to reliably attain speeds of approximately 200-1000RPM.

The motor is programmed with Rotalink's proprietary software known as Red Drive. This software allows users to program with command blocks to perform specific actions. The final test program can be seen in Figure D-2. The idea is that the motor will spin at a high enough rate to rotate the rotor, and then slow the rotor's rotation by lowering the motor's speed until it can eventually be turned off. Once the program was written and it was downloaded onto the micro-controller, 5 tests were completed to show the test ran consistently. Appendix H shows that the motor is reliable in a plot and shows the standard deviation.

Magnetic Field

In order to obtain optimum flux (surface area in contact with the magnetic field) it was necessary to implement four vertically oriented neodymium bar magnets spaced 1" inch apart in orthogonal pairs. As a result, the magnets span the entire surface area of the rotor with maximum field strength. Equation B7 shows that magnetic flux is directly proportional to the area the magnetic field travels through. Figure B-3 shows the new configuration, which will have much more area of contact to produce a greater flux.

Cylindrical, rigid polyvinyl chloride (PVC) was used as the fixture for holding the magnets around the vacutainer. The dimensions of the PVC and its geometry can be seen in Figure G-1. The purchased magnets have strong magnetic fields for their size, therefore slots matching their dimensions were cut into opposite sides of the PVC. Before being secured in place with duct tape, the magnets were placed such that the north pole of one magnet is facing the south pole of the other magnet. In addition, the inner diameter of the PVC was chosen such that the Coaxial Fluid Tester and associated components could fit within that volume.

Temperature Control

The final heating design uses a temperature controlled thermal cord laid in an aluminum structure in order to heat up to five vacutainers prior to testing. The purchased heating element uses a thermocouple and a control system to keep a given location in a set temperature range. By placing the thermocouple at the top of the aluminum housing, the thermal cord laid at the bottom of the aluminum will conduct heat through the space between these two points, bringing the samples to the required temperature. The samples are expected to remain in the required temperature range (37 - 38°C) during rotational testing, as a similar preheating process is used in state of the art blood viscometers.

Results were obtained by first placing the thermocouple at the top of the aluminum and turning the thermal cord on, so the thermal cord continued to heat until the thermocouple at the top of the aluminum was in the expected temperature range. After testing this ten times, it was found that an average of 9 minutes was required for the aluminum to reach the correct temperature throughout the assembly after starting at room temperature.

A vacutainer with 1mL of water was placed in the housing and a thermocouple was used to determine whether the liquid was also reaching the required temperature. It was found after ten trials that the water reached the required temperature after an average of 2 minutes if the aluminum block was already heated. It was then discovered that heating the liquid to 102°F is ideal, as a sample at 102°F will remain above 97°F for an average of 40 seconds during testing, as opposed to a sample heated to 98°F which only maintains adequate temperature for an average of 12 seconds.

Housing

The final enclosure design is modeled after the Rotation Assembly driving this device. Curved surfaces wrap around everything but the heating components, matching the spinning rotor that projects from the surface of the enclosure ceiling. Patterned walls add texture and allow for the walls to curve in the dual-drum shape. The enclosure is complete with a cap for the rotor insertion point to shield against overspray.

The rotational assembly is confined in the shorter, wider drum, while the tachometer and DAC are stored in the taller, thinner drum. The rotational assembly is centered in a smaller wood container which adheres to the base of the enclosure in order to keep the components in position. The tachometer is bolted to the roof of the taller drum and pointed at the top of the rotor extended out of the shorter drum. All other data collecting components have been adhered to the inside of the drum with tape, allowing them to be removed for modifications and improvements as necessary. The completed enclosure can be seen in Figure G-5.

Discussion

Verification

Incorporated Standards

There are a few standards that relate to the testing of viscosity and were considered while this project's specifications were developed. Most notably, ASTM D445^[7], Standard Test Method for Kinematic Viscosity of Transparent and Opaque Liquids (and Calculation of Dynamic Viscosity) was referenced. This standard specifies a test method for the determination of kinematic viscosity of liquid petroleum products. Although the project outlined in this proposal involves a slightly different apparatus and test substance, ASTM D445^[7] was able to explain current procedures, which helped the group determine how to proceed with the project. This allowed the group to understand the expectations of the project's stakeholders, as this product will compete with existing viscometers. ASTM F756^[8], Standard Practice for Assessment of Hemolytic Properties of Materials, was helpful in detailing one method for analyzing sample hemolysis following viscosity testing. This method utilizes a hemoglobin standard curve to compare the concentration of hemoglobin in a sample's blood plasma before and after viscosity testing.

Viscosity

In accordance with ASTM D445, the viscometer was evaluated for its repeatability and reproducibility for a variety of standard viscosity fluids^[7]. As stated in the standard, repeatability is attained when duplicate results by the same operator are within 0.35% of their mean value^[7]. Similarly, regarding reproducibility, the resulting data from different operators should be no greater than 0.7% of their mean value^[7]. As shown in Appendix H, viscosity tests with distilled water, mineral oil, and non-Newtonian standard viscosity fluids were used to benchmark the measurement consistency of the device. At this time, the prototype's outputs are not considered repeatable and reproducible with regard to ASTM D445 based on the standard deviations of measured rotor speeds. Observed differences for distilled water, low and high viscosity mineral oil are 6.8%, 3.8%, and 4.6% respectively. In order to conform to this standard, it will be necessary to improve prototype performance. See Appendix I for the appropriate testing procedure and tabulated test data.

As previously discussed, in order to measure the viscosity of blood, it is first necessary to find the speed curves for a known viscosity fluid. Distilled water, and two standard viscosity mineral oil samples were used. The motor rotated at the speeds seen in Figure H-1. For each of the 16 individual speed regions of the motor, the rotor would spin at its own individual speed depending upon the fluid tested. Each fluid was tested 10 times to produce consistent averages, and thus a characteristic curve defining the flow for the specific fluid. These curves can be seen in Figure H-2 through Figure H-5. By taking these measurement curves and applying the experimental theory discussed in detail in Appendix B, it is feasible to measure the viscosity of unknown fluids.

Testing was completed for the two samples of mineral oil and the measurement was compared to the actual viscosity given on the sample's label. Tests showed that at varying shear rates, the viscosity for the mineral oil samples stayed constant as expected by the theory. Mineral Oil A was found to have a viscosity of 4.015 cP at 20°C and Mineral Oil B was found to have a viscosity of 11.45 cP, but Figure H-6 shows that the measured viscosities were not these values. There can be numerous reasons for this measurement error but it was found that both measurements were offset by a similar factor of about 2.8. Possibly there needs to be a calibration factor to correct for certain assumptions made by the team. See Figure H-6 for a comparison plot.

When measuring the viscosity of fresh anti-coagulated blood pre-heated to 37°C (hematocrit = 48) two replicates had an average measured viscosity of 2.38 cP, at a shear rate of approximately 5 sec⁻¹. When compared to the output of a scanning capillary tube blood viscometer, it was determined that the measured value was offset by a varying factor. See Figures H-6 and H-7 for comparison plots.

Hemolysis

As detailed in ASTM F756, a standard evaluation of hemolysis is conducted based on the concentration of hemoglobin in a sample's plasma volume as compared to a baseline analysis. Additionally, hematocrit, or the ratio of red blood cells (RBCs) to plasma, is an indication of the red blood cell content and thus a measure of hemolysis. This can be measured directly using the principle of a centrifuge in devices such as the Haematokrit 210. Counting cells sorted based on their physical size can also be used to calculate the quantity of RBCs before and after testing.

Hematocrit was used to quantify hemolysis in lieu of hemoglobin content due to the availability of resources. Dr. Throckmorton in the department of Biomedical Engineering at Drexel University uses a spectrophotometer to determine the hemoglobin content of animal-derived blood samples. Unfortunately, introducing human blood into their lab space became a safety liability, requiring more time than the project deadline could allot. Thus, hematocrit was analyzed at Dr. Young Cho's lab at the Drexel Plasma Institute. A small portion of pre- and post-test sample was taken up in capillary tubes and centrifuged to visually assess the ratio of RBCs to plasma. Figures H-8 and H-9 show the results of testing.

Thermal Retention

Retaining the blood samples at a temperature of 37°C, or 98.6°F, body temperature, for the duration of the test is not essential, but highly preferred. In order to record viscosity, retaining the temperature is not necessary because the blood is anticoagulated; however, results will be more accurate if the test conditions are physiologically relevant. The method of temperature retention approached was preheating. Due to limitations within the dimensions of the system, the heating had to be done externally. An aluminum block fixture was used as the heating environment for preheating the vacutainers. The vacutainers were kept at the regulated temperature for 30 minutes until tested for heat retention, measured in time. Depending upon the starting temperature, the duration of heat retention varied. When starting at a temperature of 102°F, after 2 minutes the temperature dropped to 93°F. See Appendix I for the test protocol.

Dimension Analysis

In order to confirm that viscosity testing could be conducted uniformly using pre-fabricated glass vacutainers and rapid prototyped components, verification measurements were necessary. After measuring 50 vacutainers, the inner diameter was determined to be 0.417inch (standard deviation = 0.002inch). A small population of rotors were measured to have approximately 0.395inch outer diameter.

Magnetic Field

Due to the device's internal magnetic field, it is important to anticipate interference with regard to the device's surroundings. Static magnetic field strength was measured with a smartphone sensor on each face of the inner device housing. The magnitude in micro Tesla (uT) was recorded for all three major axes and an average magnitude of the resultant vector was calculated. Figure H-10 shows a heat map illustrating the intensity of the magnetic field at the surface of each face as well as the tabulated values. To put the numbers into perspective, the average refrigerator magnet has a strength on the order of mT^[9].

Dynamic Eccentricity

During rotation of the rotor, it is necessary that fluid contact all sides to ensure laminar flow. Figure H-11 illustrates rotor orientation during maximum rotational speed. In relation to the grid lines placed alongside the rotor, it is evident that there is no wobble or tilt of the rotor during rotation. This is due to a minimized gap ratio of 0.949 and the self-centering tendency of a vertical rotor as noted in the literature.

Eddy Current

As discussed in the theory of the creation of eddy current in previous terms as well as Appendix B, Eddy current is an induced electrical current on a non-ferrous material as a result of a changing magnetic flux through said material. The winter term verified that the rotation of magnets around the aluminum rotor created the rotational motion desired. This serves as a visual verification of the theory. By adding additional magnets closer together to increase magnetic flux, eddy current should increase and allow the rotor to spin faster. It was initially intended to verify these results experimentally by measuring the amount of current or voltage produced across the rotor, but it was determined theoretically that the magnitude of the induced voltage would be too small for the available equipment to detect. See Appendix H for detailed calculations.

Limitations

Rotor

Warping

The rotors have experienced warping due to significant fluxes in temperature. Warping has been seen to occur only at the ends of the rotor but results in great disruption when testing and recording data. It inhibits viscosity measurements due to uneven surface area contact. In some cases, the warping added friction depending upon impact of deformation. The thickness of the walls, approximately 0.005", and rotor porosity may both be factors in warping. The strongest solution is to regulate the temperature of the rotors. Other solutions include having a more durable material which may be much more expensive or thickening the walls which may affect results negatively.

Gap Ratio

The gap ratio of 0.949, ratio between the rotor outer diameter and the vacutainer inner diameter, may be too small for high viscosity fluids, causing issues during placement and interruption during subsequent rotation due to frictional forces. This issue was identified because if the rotor was sanded down on all sides to decrease the gap ratio, there was no rotational interference when testing viscous fluids.

Placement

It has been an ongoing struggle to have a proper fluid height to allow for proper rotation. If either the rotor is not placed properly, without bubbles, or the fluid height does not reach the top of the vacutainer, surface tension will not hold the rotor in place. The lubrication to allow for rotation is very specific. To solve this, more data needs to be collected to discern the optimal amount of liquid needed for sufficient rotation.

Translucency

Rare cases of erroneous tachometer readings occur due to the translucency and surface topography of the rotor material. If the infrared laser issued from the tachometer is not oriented at 90 degrees vertically and parallel with the body of the rotor, the tachometer will sometimes report incorrect values. To solve this problem, the rotor material can be changed so that it is opaque. Quick solutions include coloring it dark or using reflective tape so that the position is always perpendicular to the rotor. Angling the tachometer also seems to inhibit erroneous results.

Vibration

Vibrations have been experienced due to the high RPM of the motor. The vibration is proportional to the speed of the motor. This vibration causes the entire enclosure to shake, which causes the PVC to be offset during testing. Vibration also interferes with measurements from the tachometer and moves the cap. The strongest solution is to have optimal shock absorbing points to absorb the vibrations. Another solution is to have a stiffer material for the enclosure or to fix the entire system to a solid base.

Context & Impact

Economic Analysis

The production and implementation of medical device technologies are typically met with high production costs and numerous market restrictions due to their capacity to directly influence human wellness. The cost of these devices is often offset by the beneficial impacts they can have in both the treatment and prevention of ailments. Typical viscometers, which can serve a myriad of purposes, can also cost thousands of dollars and may not be the greatest choice for physicians looking to save money for practices and patients. Therefore it is important to devise an alternative, cost-effective means of determining blood viscosity of patients in a way that minimizes costs while preserving accuracy.

The upstream economics of this project will include the hours and research put into development of the device as well as the purchase of all necessary components. Examples of testing materials that have been and will be implemented include magnetic testing rigs, prototype housing for various elements, motor housing, and sample rotor development. Downstream economics of this project once the device has been manufactured stem primarily from sale of the device to hospitals, physicians, and researchers. In exchange for the device, consumers will receive a means of using existing materials to measure blood viscosity or that of other fluids. At this stage in the project it is difficult to determine what the final cost of the device will be, but current expenses for its development is located in the Bill of Materials (Appendix J).

Environmental Impact Analysis

There are very few environmental impacts uniquely concerning to the manufacturing and usage of this project. As with any disposable device in the medical field, the buildup of products deemed “biohazardous waste” are a concern that has plagued the industry for years. Although this device looks to incorporate elements that will contribute to this waste, these elements are not highly impactful, nor are they new developments. All disposed materials are pre-existing in the market or are of little additional material. The manufacturing of the device will follow typical industrial practices, for which it may be of interest to devise methods of cutting down on wasted energy and promoting environmentally sustainable practices.

Social Impact Analysis

In medical device development, the end goal is typically to improve the quality of human life. By developing a diagnostic or preventive tool for the medical community, physicians and patients can be alerted to concerning health factors and respond to them before they become dangerous or terminal. In the long run, this device looks to join the ranks of a list of copious other medical developments that have helped to prolong the longevity and quality of people’s lives. It is unlikely that such a device will add jobs to the market apart from their manufacturing, but it should be anticipated that such a tool will prove useful to existing occupations and research and help with their success. Since there is little mainstream awareness for the benefits of blood viscosity measurement, this device has little competition to be concerned with and, if successful, will leave a unique impact on the medical community.

Ethical Analysis

Ethical considerations are an important factor when considering any engineering concept, but require further attention in the biomedical field due to their typical direct interaction with human life. Since this device does not directly interact with the patient but instead incorporates existing technology, there is no foreseeable concern or need to acquire FDA approval.

This device looks to open new doors for preventative medicine and treatment by targeting diseases before they can begin. Diagnostic tools such as cholesterol screenings and blood pressure assessments have had a huge impact on public health and are viewed favorably as a means of determining warnings of health risks. Using the Couette flow viscometer, it is projected that blood viscosity can become the next diagnostic tool for physicians to diagnose and prevent health risks as well.

Project Management

Team Organization

Over the course of the spring term, the project maintained similar nomenclature and division that was adopted at the start of the winter term. Division of labor continued to be delegated according to group expertise and experience, but all team members were responsible for communication and support of all aspects of the project. Magnetic rotation and rotor fabrication, verification, and testing was led by Michael Sinisi. Matthew Lorenz took charge of numerous aspects of the project including all CAD design, rendering and thermal analysis for the Temperature Control element of the project, as well as manufacturing of housing and foundational support. Austin Farber continued to lead electrical aspects of the project, programming logic and implementation of software components. Dan Nguyen assisted with manufacturing and played a large role in the verification testing of various parts of the project. Richard Hanna continued his role as team manager in oversight of all aspects of the project, group dynamics, project coordination, and role assessment within the team.

Schedule and Milestones

The spring term saw many developmental changes which contrasted to different designs begun in the fall and winter terms. As anticipated, testing of the physical structure of the prototype device yielded caveats and troubleshooting requirements that were addressed hastily. This caused the team to stray from some of the initial scheduled predictions made in the winter term Gantt chart which can now be accurately depicted in Appendix L.

Group meetings between all members and the team advisor were held on Friday mornings each week with plenty of additional time spent outside of designated times. The purpose of the scheduled meetings was to update the collective team on progress, address any concerns, and focus on next steps for the week ahead. Outside time was spent continuing device development, verification testing, and troubleshooting.

Project Budget

The team is very grateful for the internal funding allotted to this project. In total the end prototype amounted to approximately \$1,650 with all components finalized. A large portion of these costs can be attributed to electrical hardware, programming logic and additional assembly components. For a breakdown of the final Bill of Materials for this project, Appendix J be referenced.

Summary & Conclusions

Over the course of the past eleven months, a viscometer based on Couette flow principles was designed in an effort to address the ever growing need for diagnostic medicine in combating cardiovascular disease. Throughout the design process, the viscometer went through numerous changes and adaptations based on new specifications and engineering constraints. Efforts to address these changes proved the capabilities of the each group member in demonstrating the creativity, organization skills, and engineering talents befitting of an exemplary design team. Although the project was met with a number of limitations, a working viscometer capable of calculating different fluidic viscosities was brought from concept, through development, to eventual completion. The device still leaves room for improvement, but can successfully be concluded in having met a majority of the stakeholder needs and specifications it set out to achieve.

Future Work

The automated Couette flow viscometer saw numerous changes, adaptations and improvements over the course of its developmental life cycle. Particular changes to note include the methods of temperature control, rotational speed, and the shift from a “coasting” motion to one that could be controlled for observing viscous behavior over varying speeds.

Although proof-of-concept of the device was achieved, there is plenty of room for improvement in future endeavors. Sizing constraints due to the necessary proximity of the magnets in relation to the ferrous rotor posed serious limitations on how other aspects of the temperature control and rotational assembly could be designed. Ideally, the temperature control system could be designed in a way that would take up minimal space and be capable of heating all areas of the test fluid equally during the analysis. However, relying on a third party heating system severely limited the ability to properly install it within the prefabricated assembly. Thus the project took a turn and had to incorporate thermal control from an exterior location as discussed previously. It would be beneficial if future designs could implement thermal control into the Rotational Assembly as originally intended.

Further standardization and verification of device characteristics must also be investigated. The team was incapable of acquiring a method of measuring magnetic field strength between the neodymium magnets and so cannot verify their effect on the aluminum rotor numerically. This could be considerably useful for improving upon rotor design and placement in the future. Additionally, determining a method for investigating hemolysis post-experimentation would be necessary to verify that the device does not pose a threat to cell structure. Possible methods discussed have included cell counting and chemical assays.

Additionally, this viscometer is currently incapable of inducing rotation under certain speeds. For investigation of non-Newtonian fluidic behaviors under exceptionally low shear forces, it would be better to investigate alternative methods than the device proposed here. The possible rotational speeds are also dependent upon the type of fluid under analysis and its associated viscosity. Higher viscosity fluids require greater rotational acceleration in order to obtain measurable data. Further investigation into controlling rotation at lower speeds than what it currently possible would be beneficial for increasing the scope of this viscometer’s capabilities.

References

- [1] Viscosity: The Unifying Parameter In Cardiovascular Disease Risk (Blood Flow Online) <http://bloodflowonline.com/commentary/blood-viscosity-unifying-parameter-cardiovascular-disease-risk>
- [2] E. Nwose, Whole blood viscosity assessment issues V: Prevalence in hypercreatininaemia, hyperglycaemia and hyperlipidaemia N Am J Med Sci. Sep 2010; 2(9): 403–408.
- [3] F. Boehning et al. (2014) Hemolysis in a Laminar Flow-Through Couette Shearing Device: An Experimental Study. *Artificial Organs* 38(9):761-765.
- [4] J. Walker et al. Fundamentals of Physics 8th Ed. Wiley, 2009.
- [5] Munson, Bruce. Fundamentals of Fluid Mechanics. 6th Edition. Wiley, 2009.
- [6] F.P. Incropera et al. Fundamentals of Heat and Mass Transfer. 6th Edition. Wiley, 2006.
- [7] ASTM D445-14e2, Standard Test Method for Kinematic Viscosity of Transparent and Opaque Liquids (and Calculation of Dynamic Viscosity), ASTM International, West Conshohocken, PA, 2014, www.astm.org
- [8] ASTM F756, Standard Practice for Assessment of Hemolytic Properties of Materials, ASTM International, West Conshohocken, PA, 2012, www.astm.org
- [9] Nevus Network. *Information on MRI Technique*. <http://www.nevusnetwork.org/mritech.htm>
- [10] Kenner, T. "The Measurement of Blood Density and Its Meaning." *Basic Research in Cardiology* 84.2 (1989): 111-24. Print.
- [11] VWR. "Monoject Blood Collection Tubes, Covidien." <https://us.vwr.com/store/catalog>
- [12] Test Standard Labs LLC. "ABS Material Data Sheet." teststandard.com
- [13] H. Zimm and D. Crothers (1962) "Simplified Rotating Cylinder Viscometer for DNA" *Proc. N.A.S.* 48:905-911.
- [14] Stratasys Objet. *Polyjet Material Datasheet*, VeraWhite. Web. 8 May 2015.

Appendix A: Needs & Specifications

Table A-1: Stakeholder needs and specifications list.

Stakeholder	Need	Priority	Specification	Metric
Senior Design Group	Automated rotational control	1	Addition of rheostat motor with control system shall slow sample rotation to 0 rpm in approximately 1 minute	55-65 seconds
Patient	Viscosity readings must be accurate.	1	Acceptable tolerances incorporated into design.	> 95% accuracy (tested against water sample)
Patient	Fast results	2	Complete results shall be observable within 30 minutes of blood collection.	</= 30 Minutes
Patient	Blood volume collection minimization	2	Amount of blood required for test shall be no more than 2 mL	</= 2 mL
Hospital	Lightweight Device	3	Complete device weight equal to or less than 10 kg (22 lb)	</= 10 kg (22 lb)
Hospital	Device Lifetime Reliability (1)	2	All moving parts to be ensured a lifetime of no less than 5 years	</= 5 years
Hospital	Device Lifetime Reliability (2)	2	All electrical components to be ensured a lifetime of no less than 10 years.	</= 10 years
Doctor/Clinic	Ease of Use (1)	2	Device shall operate with minimal user input.	</= 2 inputs required for test
Doctor/Clinic	Ease of Use (2)	2	Outputs shall consist of a graph displaying RPM vs Torsion, a calculated torsion average, and the resulting viscosity.	1 graph of RPM vs Torsion 1 Torsion average 1 Resulting Viscosity

Scientists/Experts + Doctor/Clinic	Ease of Use (3)	2	Use of device shall be sufficiently similar to existing viscometers to require little additional training.	</= 2 hours of training required
Senior Design Group	Speed Range	1	Device produces a range of rotational speeds.	0-20 RPM
Senior Design Group	Rotation Measurement	1	Device is capable of accurately measuring the shaft rotation.	95% accuracy
Senior Design Group	Manufacturability	1	Final assembly of the device must be possible at the Drexel Machine Shop.	100% completion
Senior Design Group	Temperature Regulation	1	Device must be capable of maintaining sample temperature of 36.9 C (98.4 F)	36.9 C (98.4 F)
Senior Design Group	Temperature Accuracy	1	Sample temperature must remain within +/- 0.1 C (0.18 F) of target temperature	+/- 0.1 C (+/- 0.18 F)
Doctor/Clinic	Viscosity Results Presentation	2	Viscosity must be presented in centipoise (cP or mPa*s)	100% of viscosity measurements in cP (mPa*s)
Doctor/Clinic + Scientists/Experts	Cost	3	Device must be affordable for doctors and clinics	</= \$10,000 retail
Senior Design Group	Enclosure	2	Device must be held in one enclosure for easy maneuverability and component accountability	1 solid foundation upon which all components rest

Appendix B: Detailed Theory

Viscosity

Viscosity is the measurement of a fluid's resistance to flow as defined by shear or tensile stresses within the fluid stemming from intermolecular friction. Two components are measured to characterize viscosity: dynamics and kinematics^[1]. Eq. B1 defines dynamic viscosity as a measure of the internal resistances within the fluid, relating shearing stress and fluid motion^[1].

$$\mu = \tau * \frac{dy(u)}{du} \quad [B1]$$

The second component of viscosity, known as kinematic viscosity, is defined in Eq. B2. This quantity is determined by the ratio of absolute viscosity to fluid density^[3].

$$\nu = \frac{\mu}{\rho} \quad [B2]$$

Couette Flow

Couette flow is defined as a parallel-plate flow where one plate is fixed and the other moves with constant velocity. Using the Navier-Stokes theory, the general equation governing velocity profiles can be derived^[2]. The concept of Couette flow encompasses the non-linear relationship between shear rate and fluid motion. For non-Newtonian fluids such as blood, this testing method can be used to show the direct relationship needed in order to find the viscosity of the fluid.

$$u = U * \left(\frac{y}{b}\right) + \frac{\mu}{2} * \frac{\partial P}{\partial x} * (y^2 - b * y) \quad [B3]$$

The variable u is the velocity of the fluid, b is the distance between the plates, and U is the velocity of the moving plate^[3].

$$P = - \left(\frac{b^2}{2 * \mu * U} \right) * \frac{\partial P}{\partial x} \quad [B4]$$

The value of P is a dimensionless quantity used to define the velocity profile^[3]. Figure B-1 gives a graphical and pictorial representation of both Couette flow and the behavior of a given liquid under its influence. Although many profiles can be determined from the equations above, these relationships simplify when the fluid along the moving boundary is responsible for fluid motion ($\frac{dP}{dx} = 0$)^[3].

$$u = U * \left(\frac{y}{b}\right) \quad [B5]$$

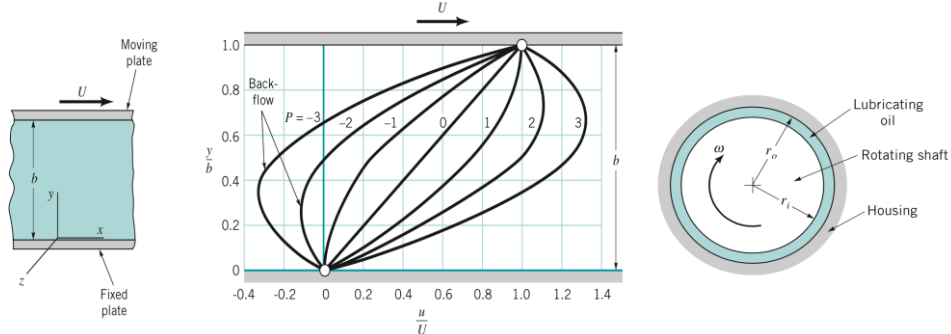


Figure B-1: Graphic representation of fluid between two plates experiencing Couette flow (left). Fluidic behavior expressed as result of Couette flow (middle). Top view of example Couette flow viscometer (right).

Viscometry

There are a number of methods used to measure a fluid's dynamic viscosity. The three most notable designs are cone-and-plate, rotating cylinder, and capillary-tube which are depicted graphically in Figure B-2. In each, the fluid is exposed to shear stress and outputs data further interpreted as viscosity. In cone-and-plate and rotating cylinder mechanisms, the system is driven by a shaft. The input torque and angular velocity are both measured^[3]. The underlying principle of capillary-tube viscometry is using the time it takes a liquid sample to fall from one defined point to another^[3].

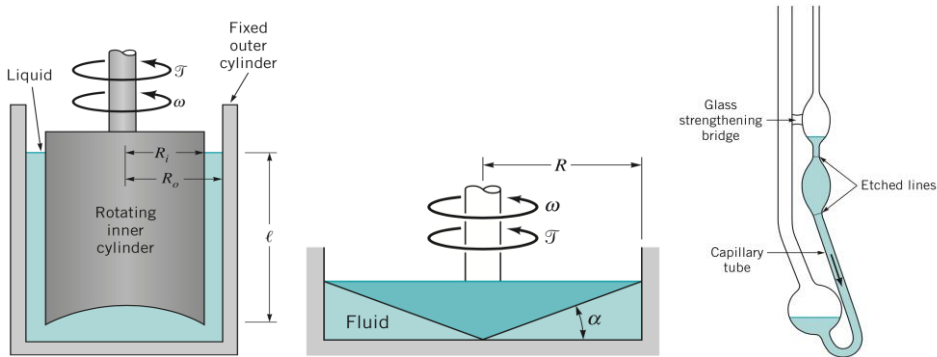


Figure B-2: Rotating Cylinder (left), Cone-Plate (middle) Viscometers, and Capillary Tube (right) Viscometers

For a Couette viscosimeter, the torque generated by the rotating inner cylinder becomes the following:

$$\text{torque} = \mu \frac{2\pi\omega LR_i^3}{R_o - R_i} \quad [B6]$$

Eddy Current

Eddy currents are circular electrical currents induced within conductors created by a changing magnetic flux. The creation of magnetic fields occur due to Faraday's law of induction, which states that magnetic fields are created due to electrical current in a direction denoted using what is commonly known as the right-hand rule^[4]. See Figure B-3 for an illustrative representation of the induced magnetic field as a result of a rotating magnet. Eq. B6 is Faraday's law and states that voltage (V) is equal to the continuous change in magnetic flux. It should be noted that the negative sign exists due to Lenz's law. Ohm's Law is also seen in Eq. B7 because voltage (V) is equivalent to current (I) multiplied with the resistance (R) travelled through. Eq. B8 is magnetic flux and is directly related to the amount of magnetic field (B) within an area (A).

$$V = -\frac{d\phi}{dt} = IR \quad [B7]$$

$$\phi = B * A \quad [B8]$$

Eddy currents can be used to create a magnetic field that opposes another magnetic field. The two fields will create a force balance, and if one field rotates, the other will rotate as well to maintain the electromechanical force balance of Eq. B7.

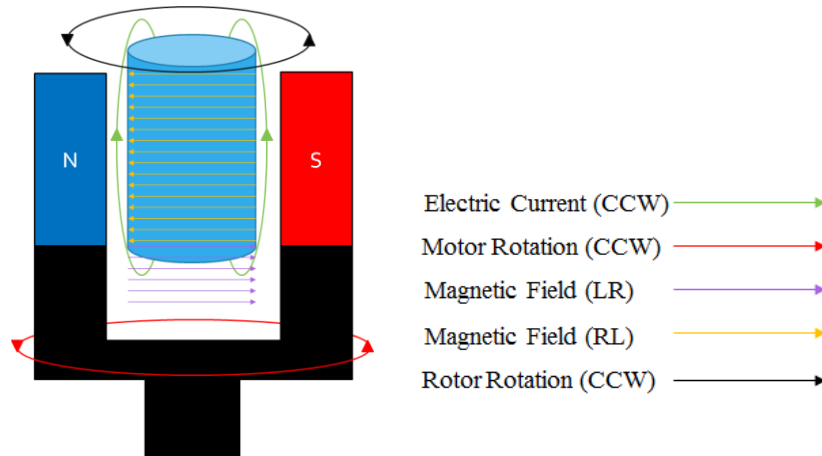


Figure B-3: Schematic of applied and induced magnetic fields due to eddy current phenomenon.

In the present system, the torque generated by the eddy current is constant at a given motor RPM. Hence, the rotor RPM will vary depending on the viscosity of the fluid at the given motor RPM. Thus yielding the following relation:

$$\mu_{water}\omega_{water} = \mu_{fluid}\omega_{fluid} \quad [B9]$$

Buoyancy

The concept of floatation stems from Archimedes' Principle of water displacement. A body submerged in fluid displaces its apparent volume and the fluid then imparts a force on the body based on the volume of fluid displaced^[5]. Eq. B10 expresses this fluid reaction force, or buoyancy force, in terms of the volume displaced (V), fluid density (ρ), and the gravitational constant (g).

$$F_b = \rho V g \quad [B10]$$

Therefore, considering that density is constant and uniform throughout the body submerged, equilibrium is established by balancing its weight and the buoyancy force. Appendix E includes theoretical calculations relying on these principles.

Heat Transfer

To maintain the body's environmental conditions during testing, the sample fluid's temperature should be maintained at 36.9°C via external preheating. Thus, it was necessary to design a container for thermal regulation. In order to determine which materials would be best suited for a thermal container, the heat transfer by conduction was determined for various materials using Eq. B11^[6]. The heat transfer by conduction (Q) is related to the thermal conductivity (k) of a given substance, along with the cross sectional area (A) of a model, the ambient temperature (T_{cold}), the desired temperature (T_{hot}), the amount of time heat is applied (t), and the thickness of the material (d).

$$Q = \frac{kA(T_{hot} - T_{cold}) * t}{d} \quad [B11]$$

It was determined that using aluminum for the body of the external heating device is most applicable due to its high thermal conductivity and ease of machinability.

Measuring Viscosity Experimentally

The first part of experimentally determining the viscosity of an unknown fluid is to gather data on a known fluid. For this testing, the motor will spin the rotor surrounded by the 1 mL water sample. Due to the motor programming, 16 individual speed regions are acquired. Due to the high consistency and low standard deviation of the testing, the average of each speed region can be acquired and used to build a new curve. The figures below demonstrate going from one curve to the next.

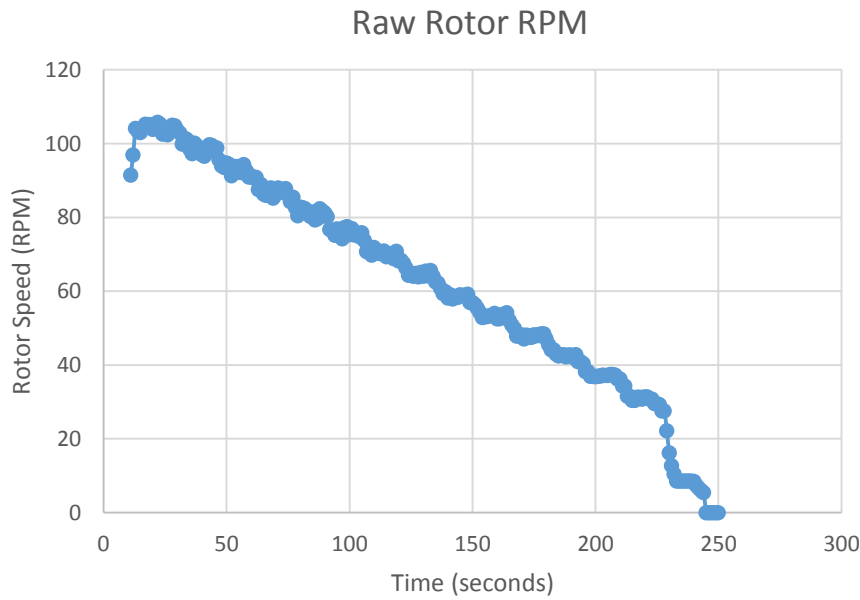


Figure B-4: Sample rotor test over different speed regions.

The black line in Figure B-4 represents the actual data, and the smaller lines are the mean value for each speed region. These means are then collected and put into a plot of speed versus speed region.

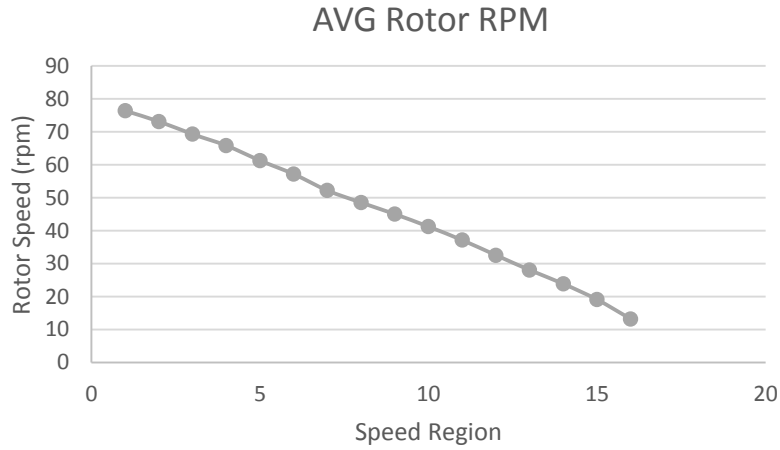


Figure B-5: Sample plot of rotor RPM output.

The straight line above can be generated for the viscosity of unknown fluids as well by performing the same test as above. Those experimental curves are presented in Figure B-6:

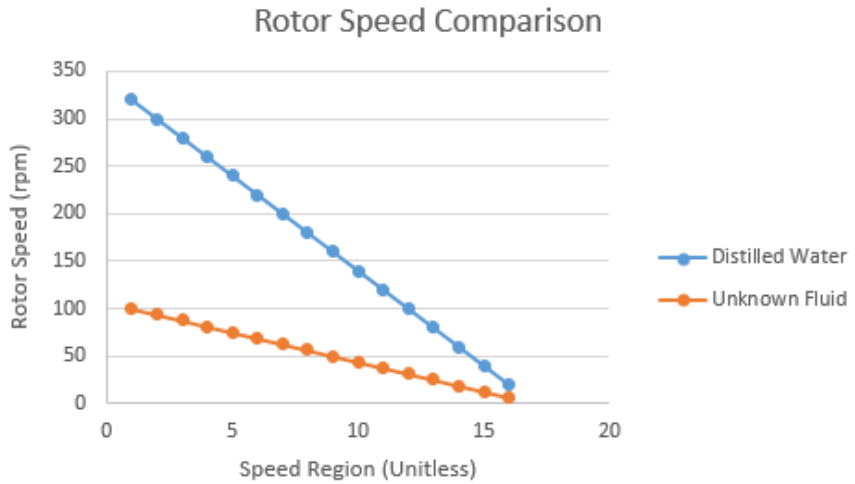


Figure B-6: Rotor speed comparisons for various fluid samples.

Equation B12 relates the RPM data of a fluid with an unknown viscosity to the known viscosity of a standard fluid, and that relationship is used as a ratio towards finding the viscosity of the unknown fluid. The equation can be used for each speed region showing the viscosity for different shear rates.

$$\frac{\mu_{\text{unknown}}}{\mu_{\text{water}}} = \frac{\omega_{\text{water}}}{\omega_{\text{unknown}}} \rightarrow \mu_{\text{unknown}} = \mu_{\text{water}} * \frac{\omega_{\text{water}}}{\omega_{\text{unknown}}} \quad [\text{B12}]$$

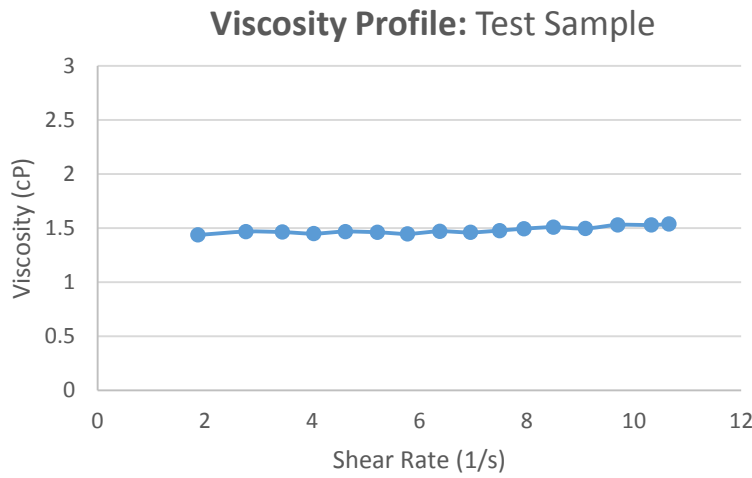


Figure B-7: Unknown fluid viscosity for various shear rates.

Equation B13 is the calculation of shear rate using measured RPM assuming a linear gap profile. The angular velocity is ω with units rad/sec and s is the ratio of the outer radius of the rotor to the inner diameter of the vacutainer.

$$\dot{\gamma} = \frac{2 * \omega}{1 - s^2} \quad [B13]$$

Appendix C: Final Assembly & Device Renders



Figure C-1: 3D Rendering of Viscometer Test Setup

DETAIL DESIGN SCHEMATIC DIAGRAM

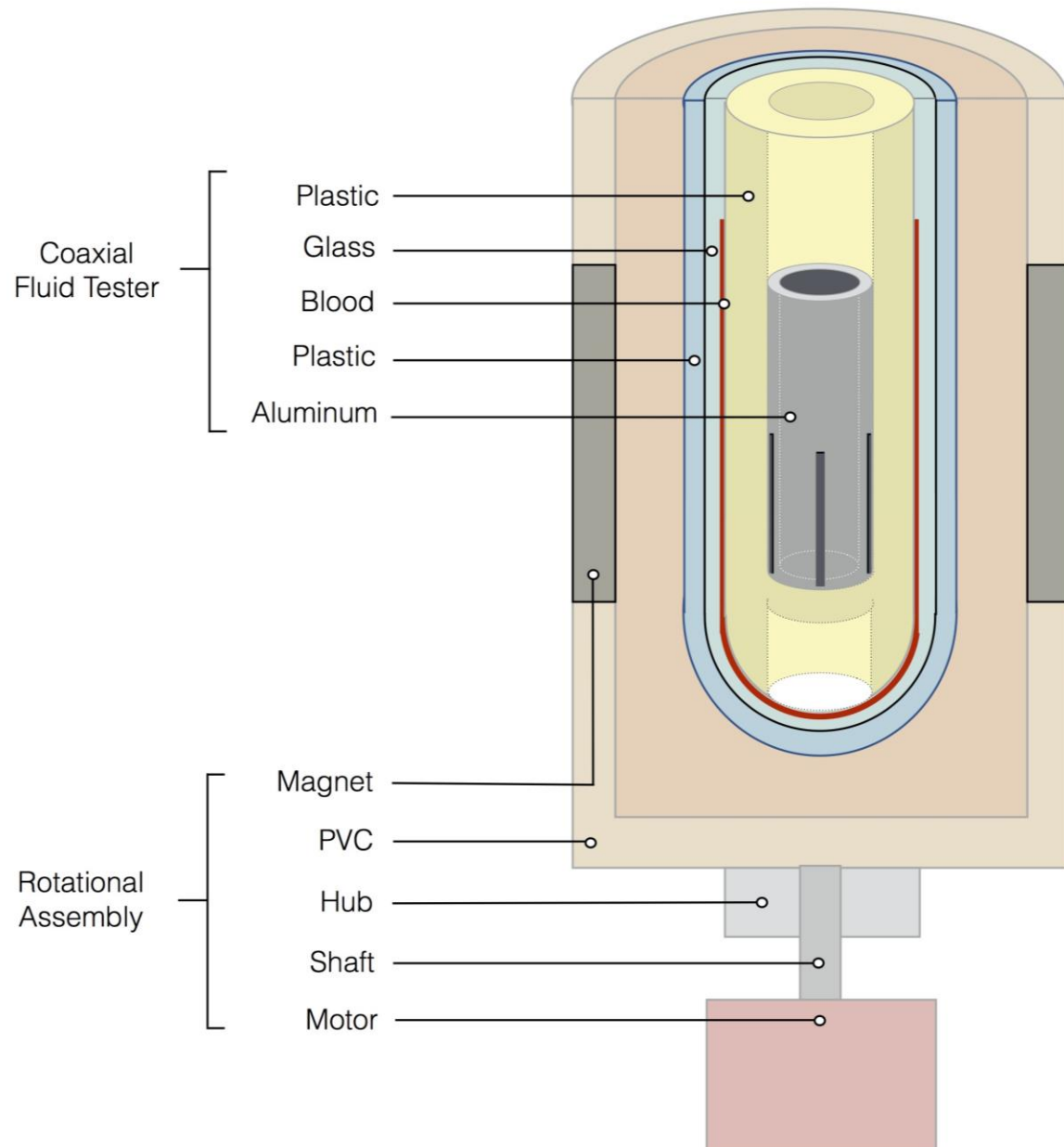


Figure C-2: Detail Device (Dissection)

Appendix D: Final Electrical Diagram & Programming Schematic

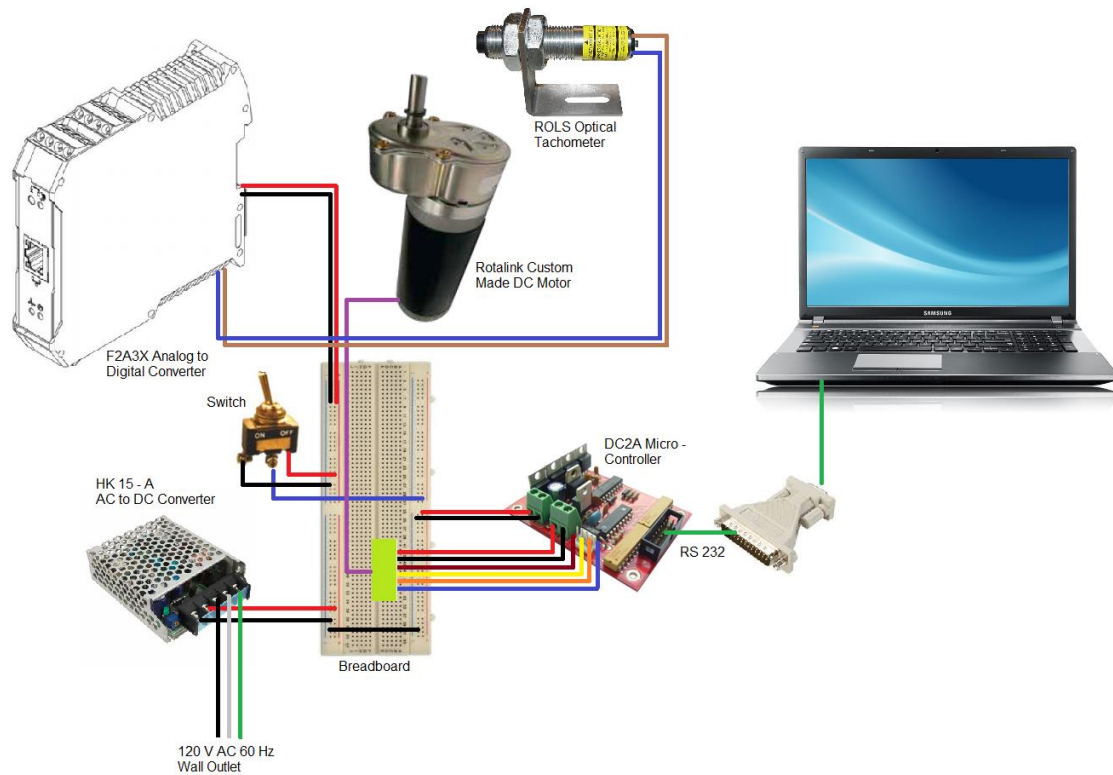


Figure D-1: Electrical schematic of all hardware

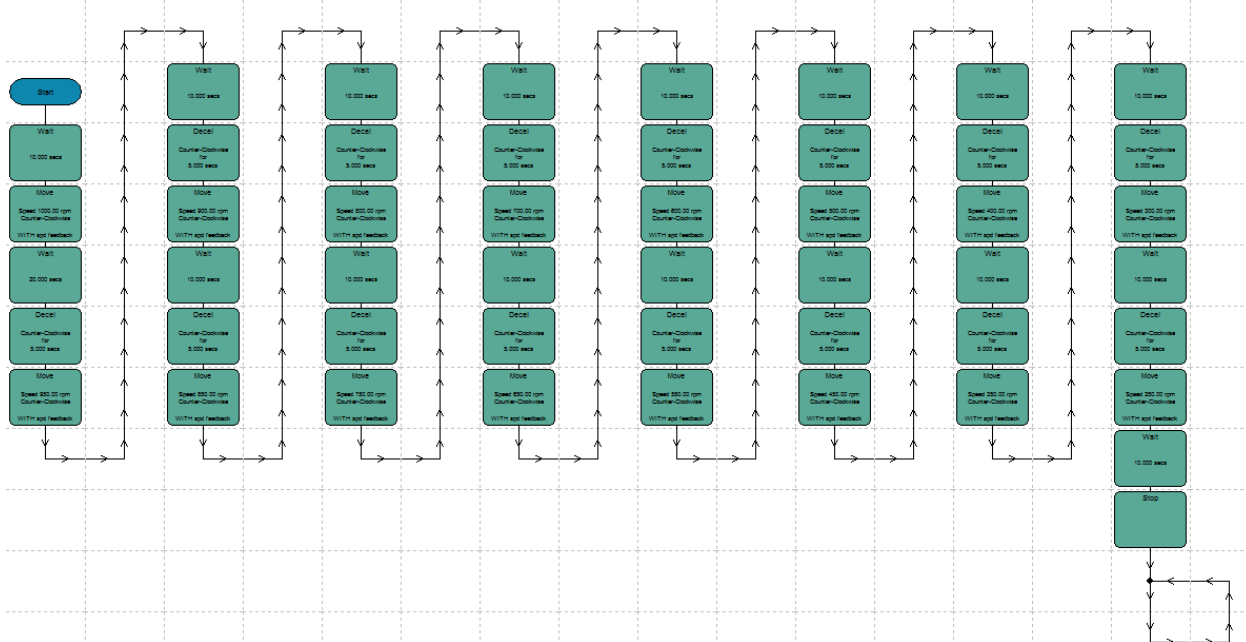


Figure D-2: Test program written for testing

Appendix E: Rotor Development & Prototyping



Figure E-1: Hybrid rotor with aluminum inserts.



Figure E-2: Aluminum and hybrid rotors.

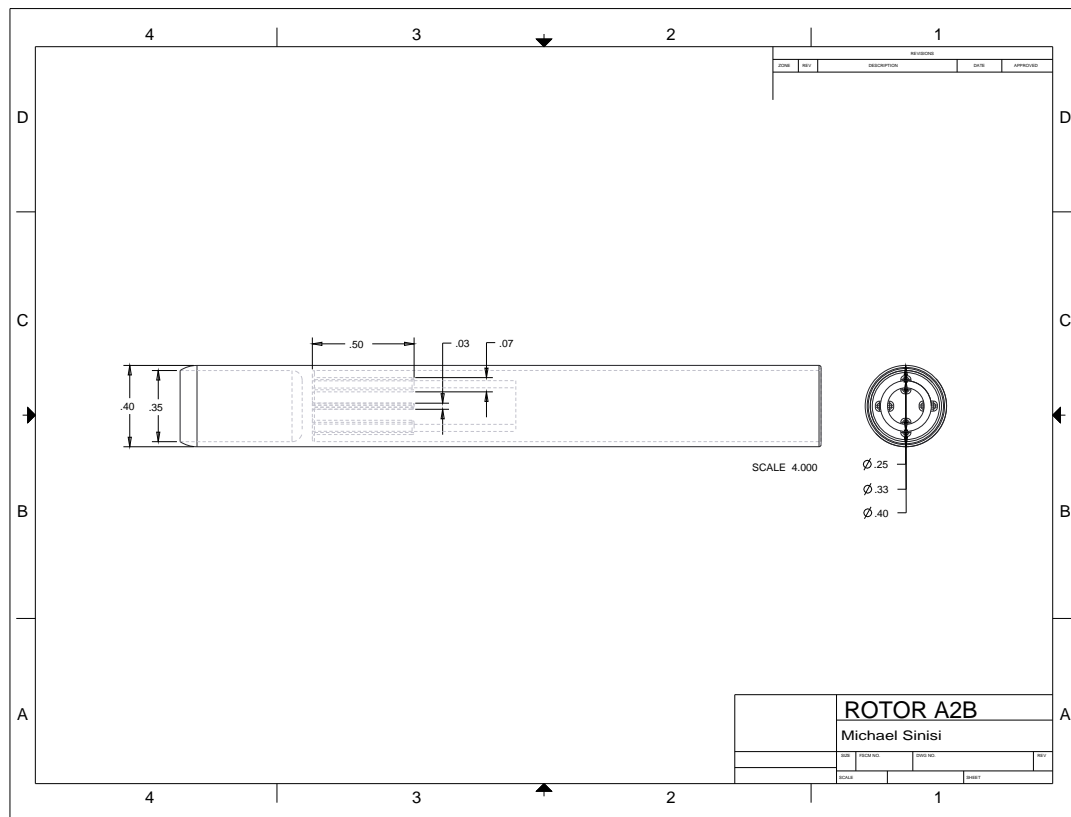
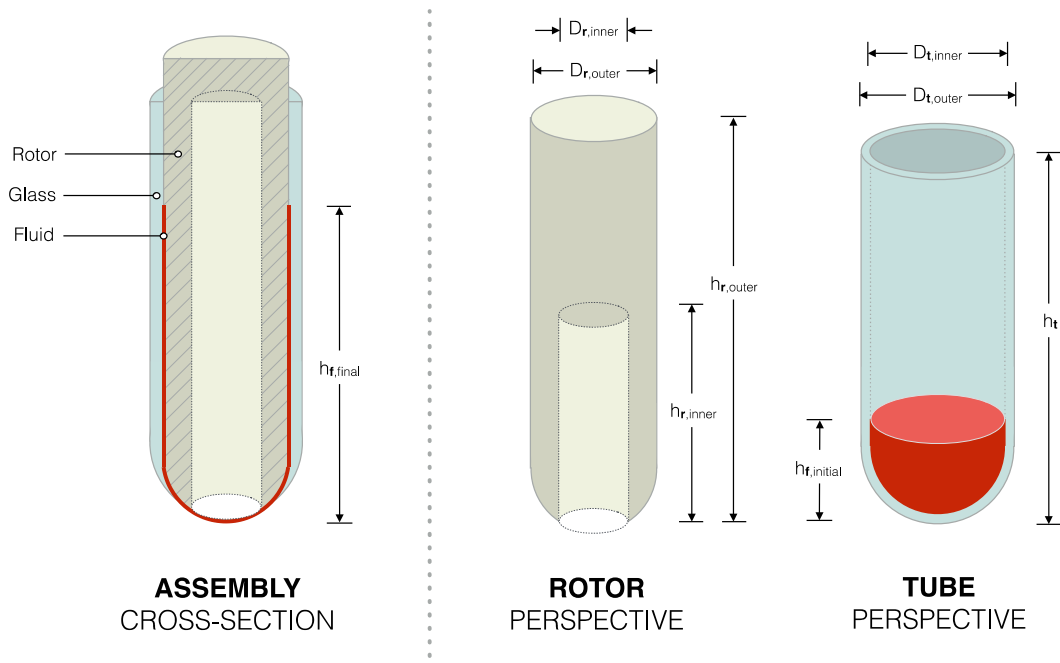


Figure E-3: Hybrid Rotor (Drawing)

BUOYANCY ANALYSIS



GIVEN

$$g = 386.4 \text{ in/sec}^2$$

$$\rho_{\text{aluminum}} = 0.102 \text{ lb/in}^3$$

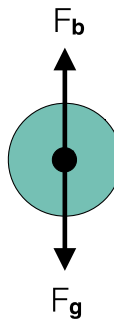
$$\rho_{\text{water}} = 0.036 \text{ lb/in}^3$$

EQUATIONS

$$F_b = (\rho_{\text{water}})(g)(V_{\text{displaced}})$$

$$F_g = (\rho_{\text{aluminum}})(g)(V_{\text{aluminum}})$$

$$F_b > F_g$$



ASSUMPTIONS

1. Rotor displaces $h_t - 0.50"$

*subtract initial height of 1mL fluid (4.5mL case)

2. Negligible rotor curvature

3. $\rho_{\text{blood}} \approx \rho_{\text{water}}$

4. $h_r,_{\text{outer}} \approx h_r,_{\text{inner}} + 0.25"$

*account for rotor interaction with tachometer

5. $D_r,_{\text{outer}} \approx D_t,_{\text{inner}} - 0.020"$

*allow for space for fluid to reside in

6. $h_r,_{\text{inner}} \approx h_t$

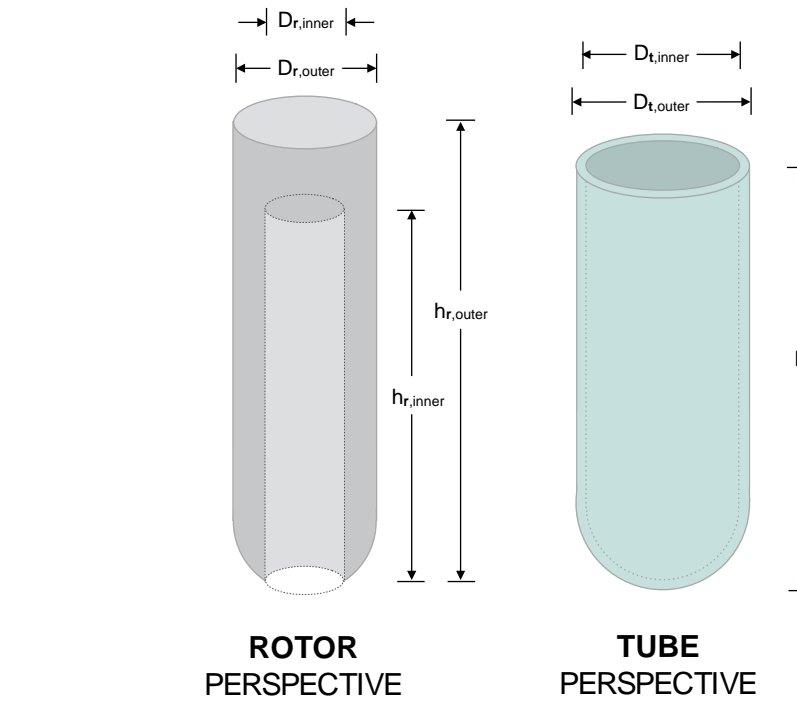
SOLUTION

$$F_b = (\rho_{\text{water}})(g)[0.25\pi \cdot (D_r,_{\text{outer}})^2](h_t - 0.50)]$$

$$F_g = (\rho_{\text{aluminum}})(g)[0.25\pi \cdot (D_r,_{\text{outer}}^2 - D_r,_{\text{inner}}^2)(h_r,_{\text{inner}}) + 0.25\pi \cdot (D_r,_{\text{outer}}^2)(h_r,_{\text{outer}} - h_r,_{\text{inner}})]$$

⇒ Use the relation $F_b > F_g$ to find the desired $D_r,_{\text{inner}}$ value.

BUOYANCY CHECK



SIZE	ROTOR					TUBE			WATER ¹		
	Vt	hr,outer	hr,inner	Dr,outer	Dr,inner	mass	ht	Dt,outer	Dt,inner	ht,water	ht,water'
10mL	4.025"	3.932"	0.506"	0.400"	0.0156 lbm	3.885"	0.600"	0.535"	0.350"	2.075"	
4.5mL	3.129"	3.034"	0.379"	0.290"	0.0310 lbm	2.890"	0.472"	0.420"	0.515"	2.050"	

¹ each experiment was measured with 1mL volume = 20 drops of water.

SOLUTION

$$F_b = (\rho_{\text{water}})(g)[0.25! \cdot (D_{r,\text{outer}}^2)(h_{t,\text{water}} - h_{t,\text{water}})]$$

$$F_g = (\rho_{\text{aluminum}})(g)[0.25! \cdot (D_{r,\text{outer}}^2 - D_{r,\text{inner}}^2)(h_{r,\text{inner}}) + 0.25! \cdot (D_{r,\text{outer}}^2)(h_{r,\text{outer}} - h_{r,\text{inner}})]$$

10mL

$$F_b = 4.82 \text{ lbm} \cdot \text{in}/\text{s}^2$$

$$F_g = 12.42 \text{ lbm} \cdot \text{in}/\text{s}^2$$

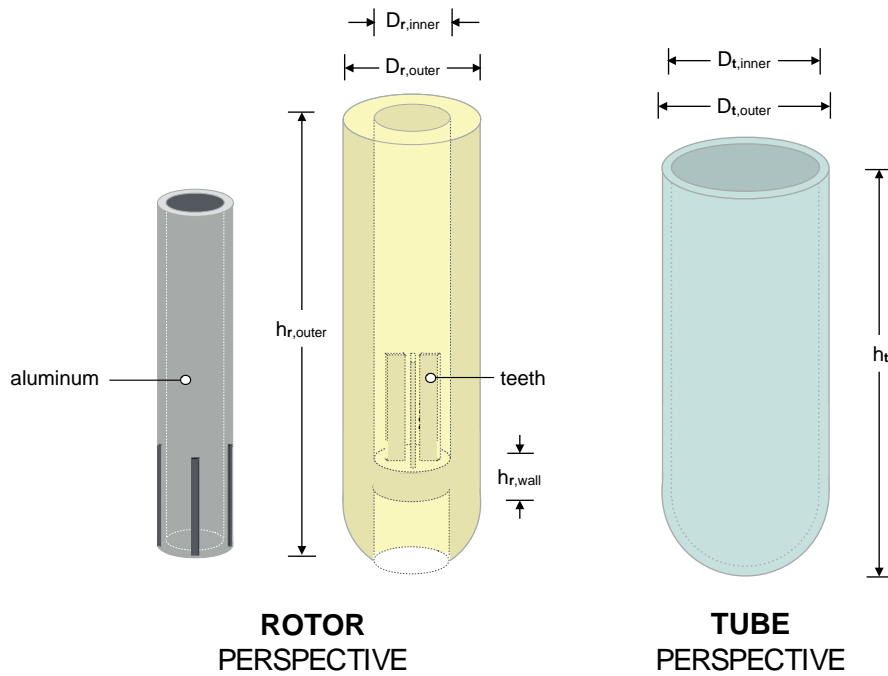
4.5mL

$$F_b = 2.41 \text{ lbm} \cdot \text{in}/\text{s}^2$$

$$F_g = 6.01 \text{ lbm} \cdot \text{in}/\text{s}^2$$

Conclusion: Changing material density to 6061 or minimizing wall thickness does not significantly reduce weight; therefore, the most feasible option is to increase the buoyancy force by either modifying the fluid's chamber or the geometry of the rotor (without increasing weight).

BUOYANCY CHECK



SIZE	ROTOR					TUBE			WATER ¹		
	V _t	h _{r,outer}	h _{r,inner}	D _{r,outer}	D _{r,inner}	mass	h _t	D _{t,outer}	D _{t,inner}	h _{t,water}	h _{t,water'}
4.5mL	3.129"	3.034"	0.379"	0.290"	0.0065 lbm	2.890"	0.472"	0.420"	0.515"	2.050"	

¹ each experiment was measured with 1mL volume = 20 drops of water.

$$*h_{r,inner} = h_{r,outer} - h_{r,wall}$$

SOLUTION

$$F_b = (\rho_{water})(g)[0.25! \cdot (D_{r,outer}^2)(h_{t,water}-h_{t,water})]$$

$$F_g = (\rho_{abs})(g)[0.25! \cdot (D_{r,outer}^2-D_{r,inner}^2)(h_{r,inner})-V_{teeth}] + (\rho_{aluminum})(g)[V_{aluminum}]$$

4.5mL

$$F_b = 3.15 \text{ lbm/in/s}^2$$

$$F_g = 2.51 \text{ lbm/in/s}^2$$

*mass used to calculate F_g

Conclusion: The hybrid-material rotor has the appropriate mass to balance the buoyancy force. The biggest challenge of this design is the lack of surface area available to induce Eddy Current; only until testing is conducted will it be clear whether the inner cylinder can drive rotation of the rotor assembly.

Appendix F: Thermal Control Development & Prototyping

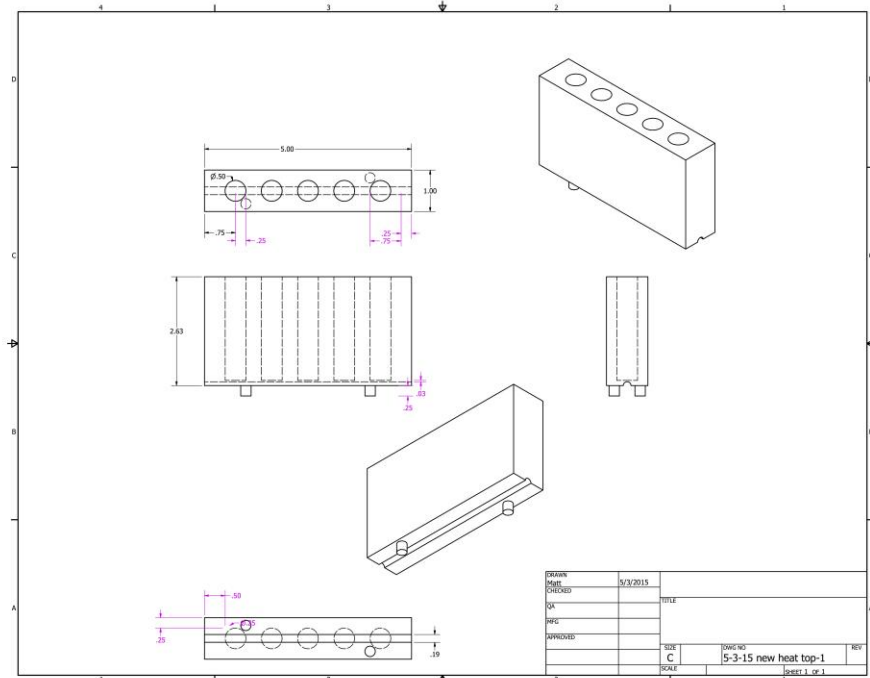


Figure F-1: Vacutainer Heating Fixture Body (Drawing)

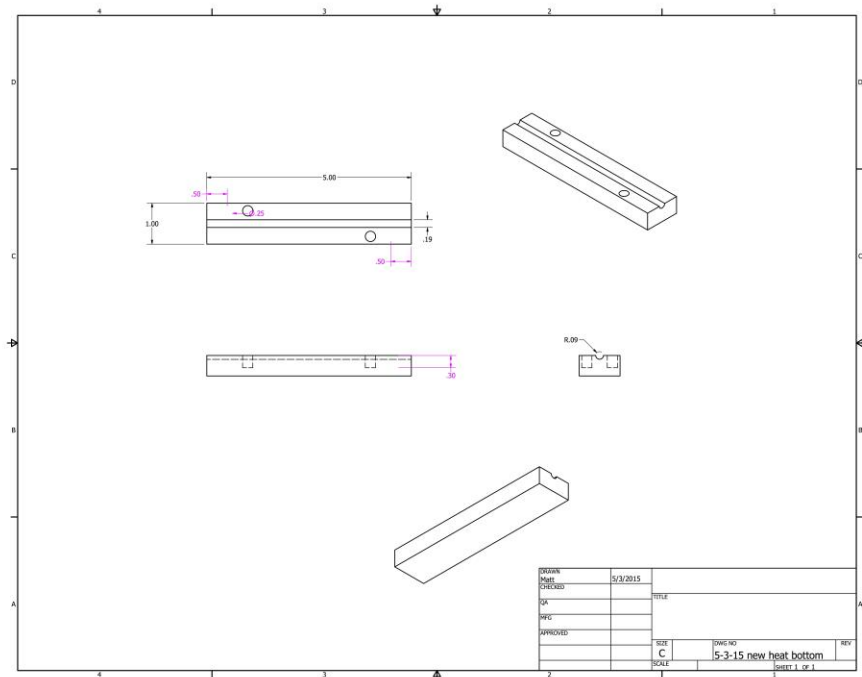


Figure F-2: Vacutainer Heating Fixture Base (Drawing)

Appendix G: Housing Development & Prototyping

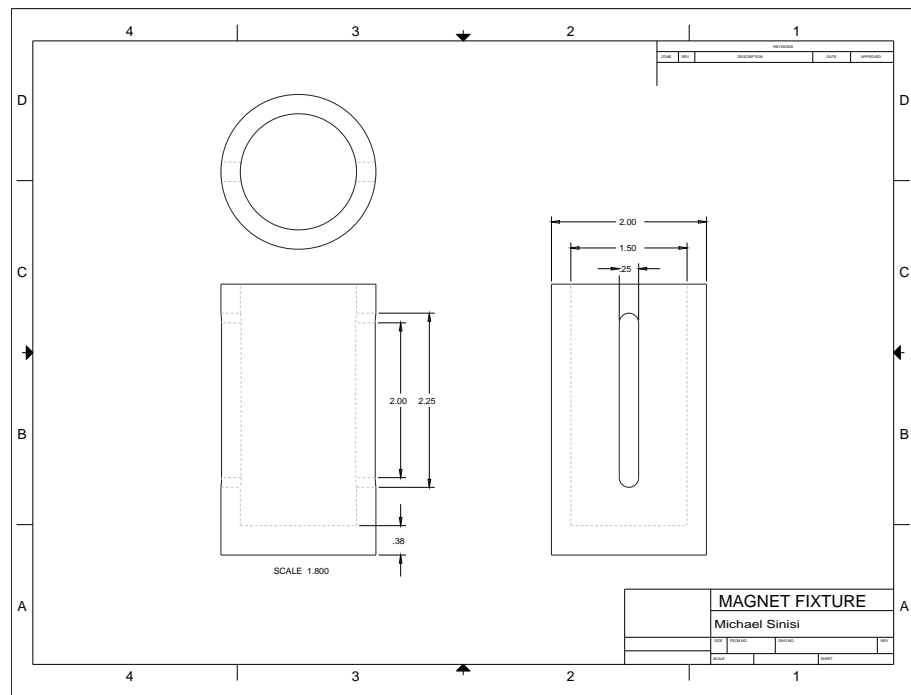


Figure G-3: Magnet Fixture (Drawing)

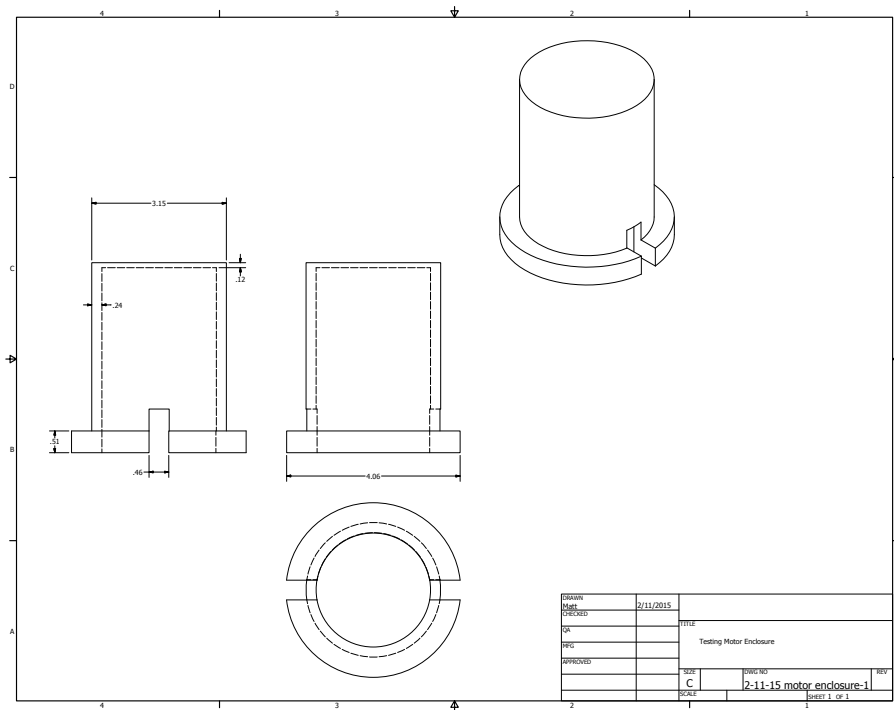


Figure G-6: Motor Enclosure (Drawing)

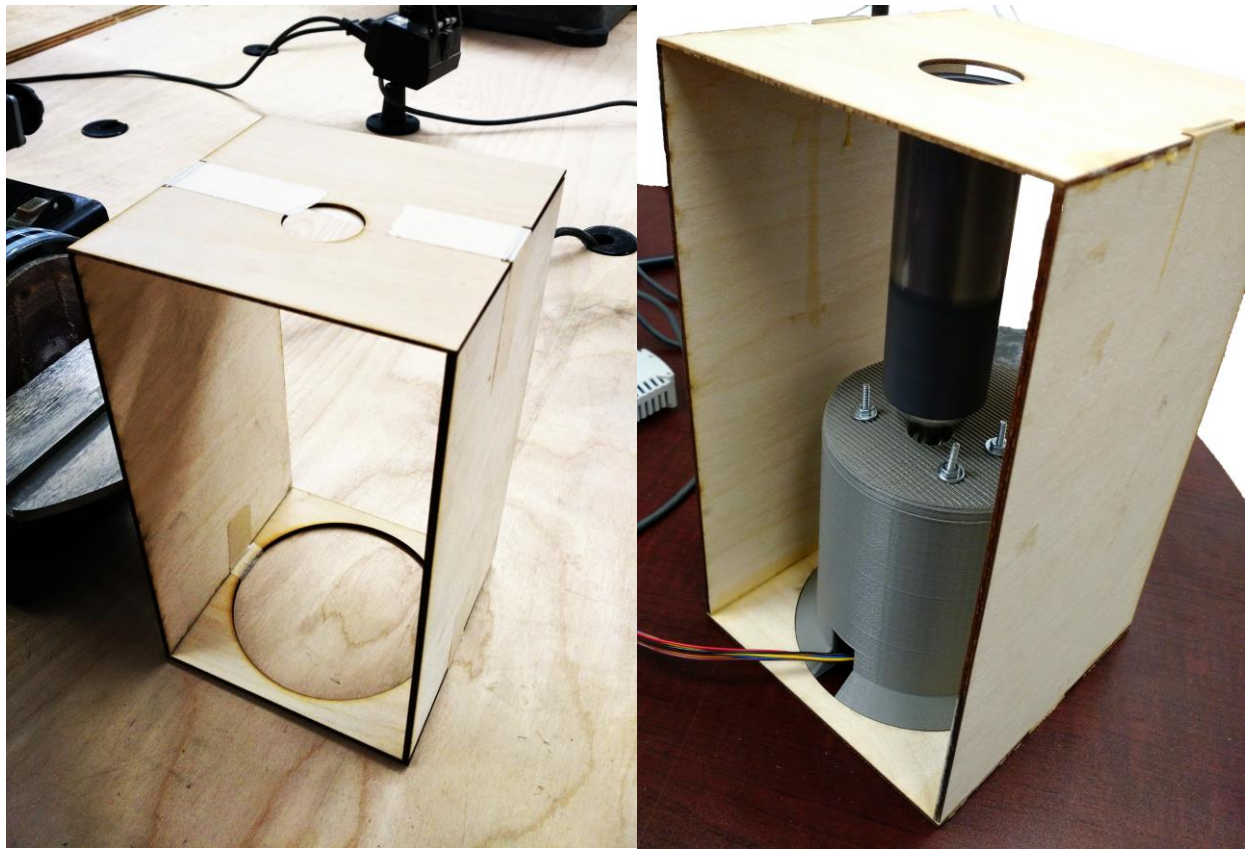


Figure G-3: Wooden inner housing prototype.

Figure G-4: Final prototype inner housing assembly



Figure G-5: Full device assembly

Appendix H: Experimental Results

Viscosity Measurements

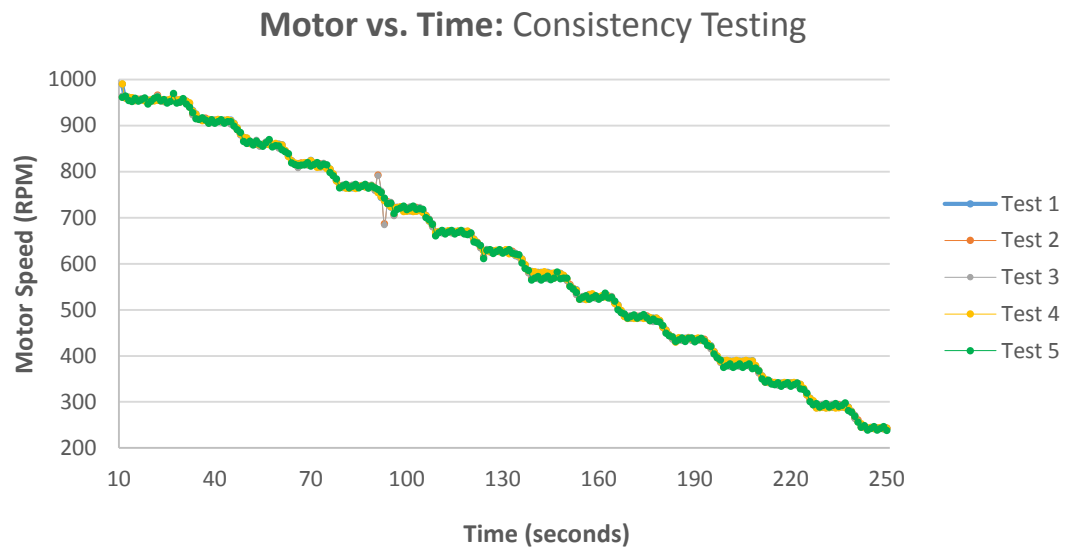


Figure H-1: Consistency Test Data for Motor

Table H-1: Consistency Test Data Mean and Standard Deviation

Speed Region	Mean Speed					Standard Deviation of Speed					Mean	Standard Deviation in Speed Region
	Test 1	Test 2	Test 3	Test 4	Test 5	Test 1	Test 2	Test 3	Test 4	Test 5		
1	958.417	956.803	956.362	958.249	956.523	7.76616	4.47157	4.414	8.11364	5.78114	957.271	6.109302697
2	912.422	910.086	909.402	912.142	910.004	0.37389	3.27213	3.38428	1.25038	3.84099	910.811	2.424333514
3	860.391	860.802	860.118	860.111	860.72	1.22331	4.44934	5.50569	1.39556	5.41039	860.428	3.596855971
4	815.626	815.756	815.072	815.346	815.674	5.209	2.6051	3.89831	5.42583	2.66806	815.495	3.961260512
5	766.887	768.535	767.851	766.607	768.453	1.51261	2.50668	3.80965	2.06272	3.38782	767.667	2.655895323
6	717.203	719.824	719.14	716.923	719.742	4.12008	5.25819	6.2952	4.37035	4.54546	718.566	4.917854954
7	670.458	668.395	667.711	670.178	668.313	1.3469	2.23623	2.94224	1.78481	3.45375	669.011	2.352786479
8	625.502	625.779	625.095	625.222	625.697	4.28726	3.77742	4.37232	4.43535	4.23051	625.459	4.220570603
9	578.611	570.385	569.701	578.331	570.303	4.38815	3.29878	3.65447	4.51761	4.93131	573.466	4.158063923
10	527.851	527.25	526.566	527.571	527.168	5.49501	4.41971	5.17638	5.8598	4.847	527.281	5.159581833
11	480.277	480.407	479.723	479.997	480.325	5.95916	7.7606	7.99668	6.16864	7.31735	480.146	7.040484926
12	435.028	432.951	432.267	434.748	432.869	5.71356	6.85725	7.25213	5.79176	6.66001	433.573	6.454940288
13	386.387	377.23	376.546	386.107	377.148	6.96124	4.77544	5.5199	7.05036	5.11575	380.684	5.88454003
14	337.637	334.805	334.121	337.357	334.723	8.17762	7.41472	7.8927	8.29528	7.39967	335.729	7.83599802
15	285.719	288.73	288.046	285.439	288.648	6.30234	9.57394	9.85744	6.37161	9.51153	287.316	8.323371278
16	243.73	243.258	242.184	243.282	242.796	0.14335	0.16634	2.04693	0.99803	3.93064	243.05	1.457060109
				Standard Deviation in Test	4.31123	4.55272	5.25114	4.61823	5.18946			

Speed Curves for Distilled Water

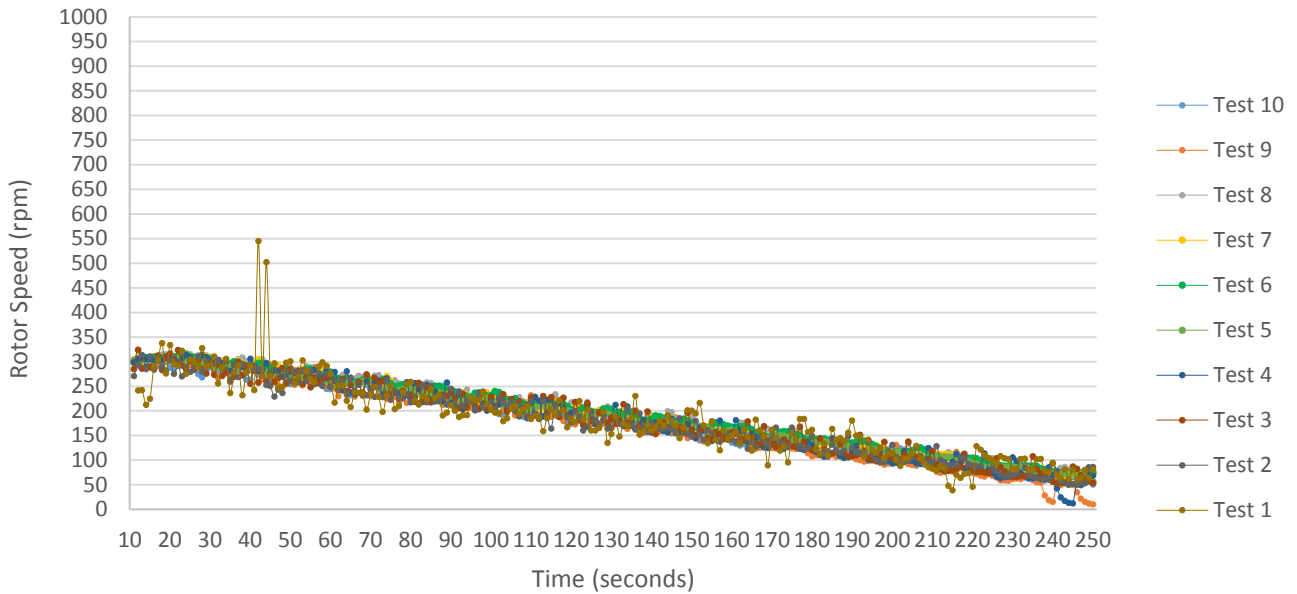


Figure H-2: Speed curve data for distilled water showing consistency.

Table H-2: Tabulated distilled water speed curve data.

Speed Region	Mean Speed										STD of Speed										Mean	STD in Speed Region
	Test 1	Test 2	Test 3	Test 4	Test 5	Test 6	Test 7	Test 8	Test 9	Test 10	Test 1	Test 2	Test 3	Test 4	Test 5	Test 6	Test 7	Test 8	Test 9	Test 10		
1	287.1	292.3	297.2	306.3	303.1	309.3	306.1	312.4	302.4	289.77	35.14	12.43	14.38	4.104	3.5277	2.4413	6.547	3.7672	5.7238	8.0831	300.59	9.6098
2	320.7	278.8	274.8	290.4	286.2	293.9	292.7	300.4	285.8	272.61	109.3	16.25	14.52	9.538	5.7486	4.1317	8.4176	5.6565	10.111	9.2495	289.63	19.288
3	279.2	267.2	261.5	275	268.1	278.8	277.7	282.8	270.4	259.32	16.62	13.43	9.866	7.31	4.4453	4.0287	4.6098	5.2113	15.714	10.187	272	9.1428
4	230.7	239.8	250.6	247.3	251.7	261.3	260.3	266.1	242.8	245.57	17.36	12.97	15.02	14.93	7.5712	3.4744	7.0555	5.8037	19.726	11.085	249.61	11.5
5	219.5	229.2	232	236	235.9	246.9	242.1	253.4	225.2	231.12	16.32	14.66	12.72	16.61	4.416	5.1068	4.9459	4.9618	12.426	7.8406	235.12	9.9999
6	206.3	215.9	217.6	214.7	220.2	232.3	224.4	227.7	210.2	210.92	17.93	10.45	14.14	10.35	6.4628	6.0198	6.3177	9.1396	11.474	12.339	218.01	10.463
7	189.4	193	202.6	208.8	204.6	213.4	208.8	218	198.4	194.24	17.79	15.86	19.66	15.57	5.4426	4.5839	7.5236	8.0364	18.165	13.972	203.12	12.66
8	168.2	177.8	183.5	186.8	188	199.1	195.8	198.9	179.7	184.79	19.69	11.78	13.04	15.55	7.2631	3.743	5.8259	6.8822	11.164	7.93	186.25	10.288
9	177.6	163.9	169.3	166.2	171.6	182.8	176.8	184.7	162.8	165.4	17.23	10.32	11.8	11.17	6.3316	4.7797	5.658	8.1832	13.23	10.169	172.1	9.8875
10	143.7	143	151.7	154.1	154.7	169.6	163.4	162.7	143.6	147.89	15.27	11.57	11.23	15.91	6.5336	4.0594	3.2252	8.9201	10.518	15.39	153.44	10.263
11	147.3	139.7	134.3	131.8	141.8	150.9	146.9	146.7	126.2	134.02	27.74	15.94	13.69	11.06	8.1991	6.357	7.2501	8.3239	10.582	10.563	139.96	11.97
12	143.4	122.4	116.8	111.2	124.7	136.5	131.8	131.6	107.2	119.12	19.44	11.78	15.01	8.865	5.346	2.0292	1.803	5.1108	7.8284	15.959	124.47	9.318
13	101	103.5	109	102.5	109.6	119.2	111.2	113.2	97.66	103.96	14.04	9.69	12.18	11.07	5.7406	4.3227	1.4784	9.969	14.069	14.291	107.09	9.6847
14	89.54	95.63	84.01	88.44	93.85	100.8	97.05	99.5	79.83	96.109	27.42	8.69	11.46	14.36	7.3251	5.1169	8.3587	3.8463	14.815	11.437	92.479	11.283
15	90.31	74.49	72.18	71.66	79.37	85.36	80.19	77.07	50.91	62.547	11.64	14.51	14.38	12	5.7224	4.4898	4.1433	4.1042	21.999	4.1857	74.407	9.7182
16	64.77	56.34	42.52	41.09	57.55	59.57	62.63	55.98	13.17	39.692	11.33	21.21	25.95	22.76	11.832	22.892	11.543	21.628	9.2328	22.873	49.332	18.124
	STD in Test										24.64	13.22	14.31	12.57	6.3693	5.4735	5.9189	7.4715	12.924	11.597		

Speed Curves for Mineral Oil A

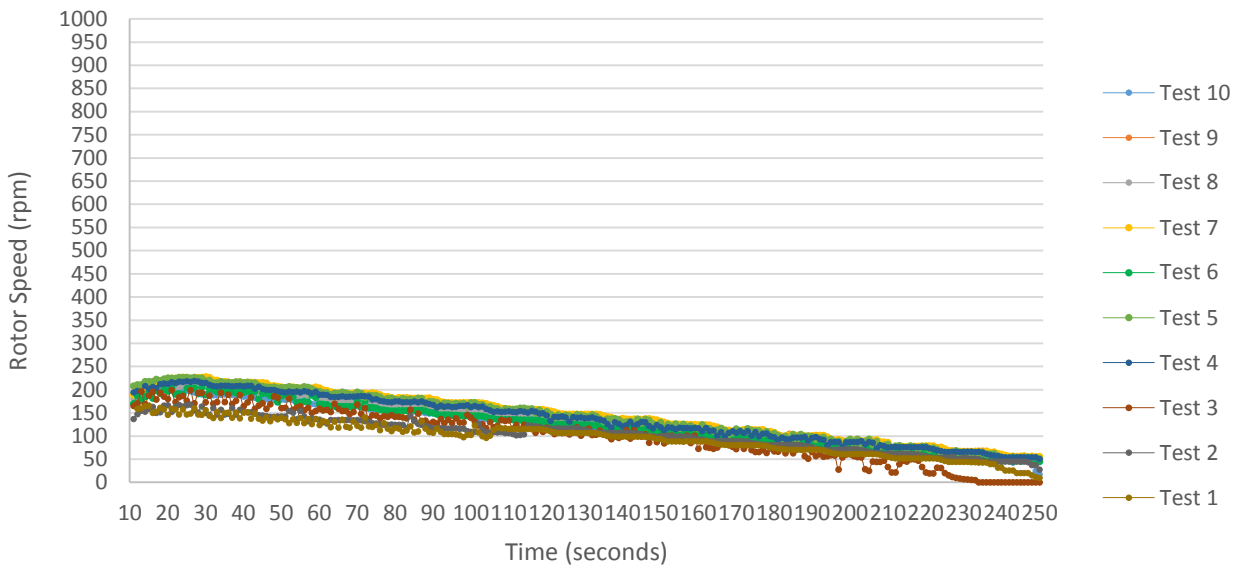


Figure H-3: Speed curve data for Mineral Oil A showing consistency.

Table H-3: Tabulated Mineral Oil A speed curve data

Speed Region	Mean Speed										STD of Speed										Mean	STD in Speed Region	
	Test 1	Test 2	Test 3	Test 4	Test 5	Test 6	Test 7	Test 8	Test 9	Test 10	Test 1	Test 2	Test 3	Test 4	Test 5	Test 6	Test 7	Test 8	Test 9	Test 10			
1	155	158.6	184.6	211.7	222	194.2	218	201.7	216.2	196	6.645	7.148	10.31	7.19	5.0898	8.3224	11.295	7.9622	9.4981	3.5472	195.79	7.7012	
2	143.9	150.7	174.3	207.1	214.3	193.7	215.9	197.8	214.2	185.7	7.18	5.164	10.44	2.529	3.3768	5.0514	0.7331	1.393	1.4373	3.818	189.76	4.1124	
3	132.1	142.4	160.8	194.5	203.3	179.8	204.9	187.1	202.4	174.23	5.592	7.961	8.385	2.24	3.5124	7.827	0.9286	1.9974	1.0993	4.4432	178.14	4.3985	
4	125.2	132.7	151.1	184.5	190.2	165.5	192.6	175.5	190.4	163.09	7.842	2.926	8.693	2.665	3.6433	5.4931	0.4702	1.36	1.7143	4.1305	167.07	3.8937	
5	114.3	125.2	138.6	172.6	178	154.2	182	165.1	178	153.24	7.824	7.89	8.922	2.487	3.5383	1.935	1.1322	1.51	1.196	3.2281	156.12	3.9662	
6	103.8	113.6	131.1	162.9	168.2	143.4	171.4	155	168.1	143.26	7.663	5.754	8.423	3.44	3.5754	1.9633	1.4939	1.5292	1.5798	5.1529	146.07	4.0573	
7	115	113.4	117	151.2	156.2	134	157.7	144.2	155.7	132.92	1.021	8.929	5.629	3.042	4.4513	1.9323	0.6377	2.3684	1.5067	4.254	137.72	3.377	
8	106.3	112.1	108.7	137.8	141.9	123.7	147	133.4	143.6	122.78	1.407	4.006	6.627	3.222	4.7277	2.0501	1.1984	2.2208	1.325	4.3147	127.74	3.1099	
9	97.83	103.1	99.72	124.5	130.9	114.3	136.1	121.8	133	111.12	2.125	3.537	8.903	4.77	4.3932	2.8705	1.46	2.1903	1.9969	5.009	117.25	3.7255	
10	87.92	93.37	84.15	114	118.5	103.8	124	112.3	122.3	101.49	1.897	3.925	11.4	5.324	4.7551	2.0063	1.7274	2.8025	2.3841	4.0007	106.18	4.0222	
11	79.22	84.35	72.11	104.7	109.6	94.44	112.4	101	110	91.267	2.262	3.581	7.912	4.911	3.9745	2.7976	2.1534	2.6478	2.5363	4.4588	95.911	3.7234	
12	69.73	75.24	60.95	93.01	96.78	84.4	100.3	90.43	96.79	81.605	2.419	4.202	7.434	5.753	4.106	3.5518	2.7233	2.6766	2.921	4.0334	84.926	3.9821	
13	60.27	66.41	43.47	82.82	85.2	74.01	89.95	79.64	87.02	71.18	2.029	3.814	11.15	5.667	5.5104	3.873	1.876	3.176	3.1734	4.4867	73.997	4.4759	
14	51.06	56.78	32.52	73.07	73.01	64.43	77.46	69.58	75.38	59.793	1.757	3.483	12.52	3.883	5.7318	3.9705	2.276	2.5883	2.6389	3.775	63.31	4.262	
15	40.57	47.84	1.824	62.2	61.24	54.2	65.6	59.17	64.98	50.051	4.811	3.195	2.951	4.289	3.718	3.7308	2.4755	2.9304	3.4458	3.739	50.768	3.5287	
16	11.3	32.08	0	47.28	45.33	41.73	52.76	41.08	49.41	22.986	5.703	8.068	0	8.435	13.239	7.9117	6.2602	15.021	6.5626	16.563	34.395	8.7764	
											STD in Test	4.261	5.224	8.107	4.365	4.8339	4.0804	2.4276	3.3984	2.8135	4.9346		

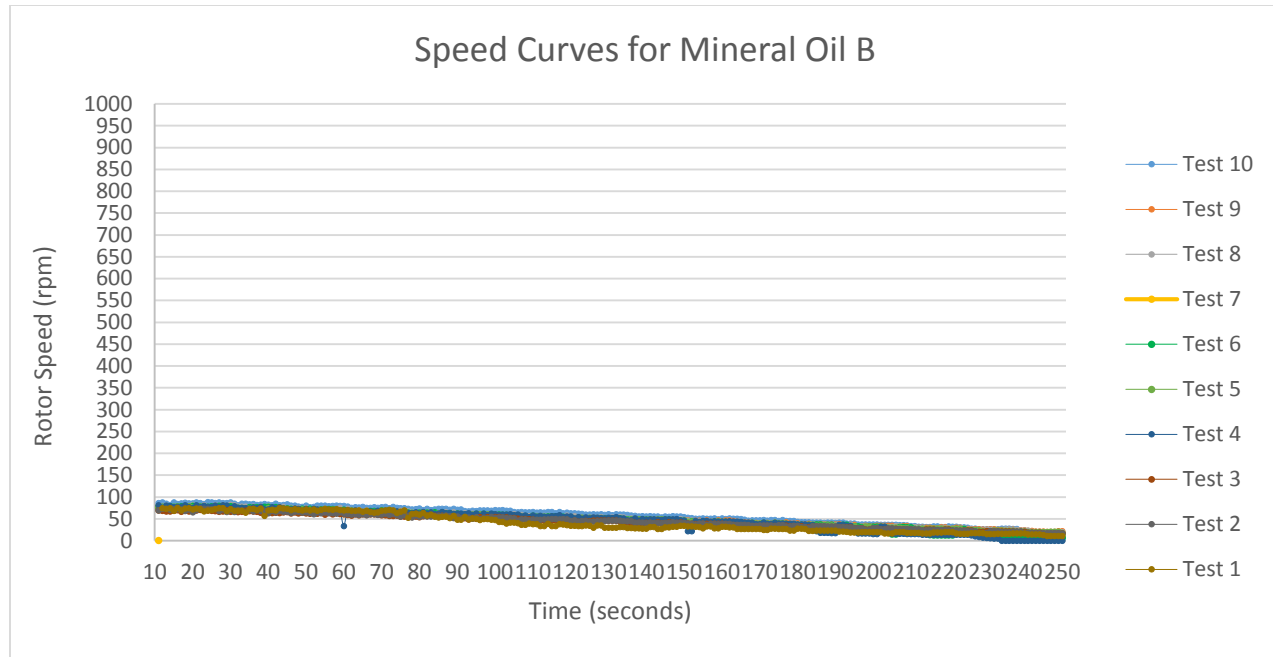


Figure H-4: Speed curve data for Mineral Oil B showing consistency.

Table H-4: Tabulated Mineral Oil B speed curve data

Speed Region	Mean Speed										STD of Speed										Mean	STD in Speed Region
	Test 1	Test 2	Test 3	Test 4	Test 5	Test 6	Test 7	Test 8	Test 9	Test 10	Test 1	Test 2	Test 3	Test 4	Test 5	Test 6	Test 7	Test 8	Test 9	Test 10		
1	72.33	71.45	68.85	78.54	79.53	75.84	77.06	79.03	74.77	86.515	2.613	2.569	1.425	2.12	2.0194	2.0364	1.8423	2.2043	1.8447	1.6989	76.391	2.0373
2	70.81	67.48	65.21	74.78	75.16	71.43	74.79	76.6	72.18	82.963	5.108	2.16	1.253	2.08	1.9974	2.2842	1.9032	2.0984	1.8658	1.2958	73.141	2.2047
3	71.07	63.46	62.86	66.83	71.02	68.24	70.2	71.76	67.93	79.634	1.305	1.488	1.93	11.58	1.7071	2.3259	2.1767	2.1759	1.3195	1.393	69.3	2.7405
4	67.59	59.59	58.78	66.18	66.25	64.48	66.43	68.31	64.54	76.133	2.524	1.89	1.669	1.864	1.3948	2.0649	1.9065	1.5155	1.7221	1.2678	65.83	1.7819
5	56.08	56.28	55.94	63.36	62.29	59.9	62.1	63.96	61.14	72.071	4.299	1.731	1.858	1.755	1.7425	2.3417	1.6814	1.5029	1.3439	1.2432	61.311	1.9499
6	45.45	52.76	53.19	60.12	59.08	56.65	58.61	59.53	57.17	69.17	3.813	1.376	0.974	1.623	2.0478	2.1312	1.1897	1.6135	1.5405	1.2913	57.173	1.7601
7	35.86	48.77	46.94	56.12	53.95	52.74	54.44	55.77	53.08	64.576	2.11	1.383	0.915	1.237	1.7154	1.4418	0.9268	1.5513	1.1263	1.1222	52.225	1.353
8	31.26	45.32	45.28	51.8	49.42	49.06	49.98	52.28	50.7	60.221	2.066	0.951	1.579	1.903	1.5991	1.6079	1.1631	1.6279	1.3045	0.878	48.532	1.468
9	31.16	41.34	41.09	48.66	45.21	45.56	46.67	47.58	47.68	55.53	2.515	0.661	1.148	1.057	1.7545	2.2755	0.9918	1.553	0.9569	0.8187	45.048	1.3733
10	30.46	37.95	37.23	44.3	40.72	41.4	41.84	43.16	44.84	50.531	2.409	1.136	2.158	0.686	1.6964	2.01	0.5736	1.4642	1.9197	0.8405	41.243	1.4893
11	26.16	34.49	33.55	39.45	37.06	37.43	38.03	38.67	40.49	46.204	1.672	1.143	0.643	1.16	1.8681	2.1698	1.4926	1.0878	1.1072	1.3869	37.153	1.3731
12	21.82	32.14	30.87	25.53	33.54	33.38	34.4	35.91	37.16	41.12	1.9	1.472	0.834	8.82	0.4645	1.1009	1.8478	1.3321	1.1085	1.0293	32.586	1.9908
13	18.72	27.62	26.19	20.11	29.97	29.04	26.68	32.35	33.84	36.324	1.513	1.061	1.143	6.915	1.4324	1.47	6.6442	1.0464	1.1073	1.103	28.086	2.3436
14	18.16	24.39	23.86	14.24	25.64	25.86	18.35	27.82	28.91	31.768	1.382	0.958	1.188	0.07	1.1873	1.7525	6.5261	1.2499	1.2923	0.9808	23.9	1.6587
15	16.43	20.85	21.14	1.68	22.84	21.78	11.53	24.35	25.14	25.492	0.645	1.191	0.61	2.716	1.4879	1.0817	0.333	1.1402	0.7712	3.7659	19.123	1.3742
16	10.95	16.56	14.52	0	18.15	14.28	6.347	19.74	20.28	11.551	0.317	1.538	3.25	0	0.6903	5.2925	0.6312	1.3981	1.2876	0.1475	13.237	1.4552
	STD in Test										2.262	1.419	1.411	2.849	1.5503	2.0867	1.9894	1.5351	1.3511	1.2664		

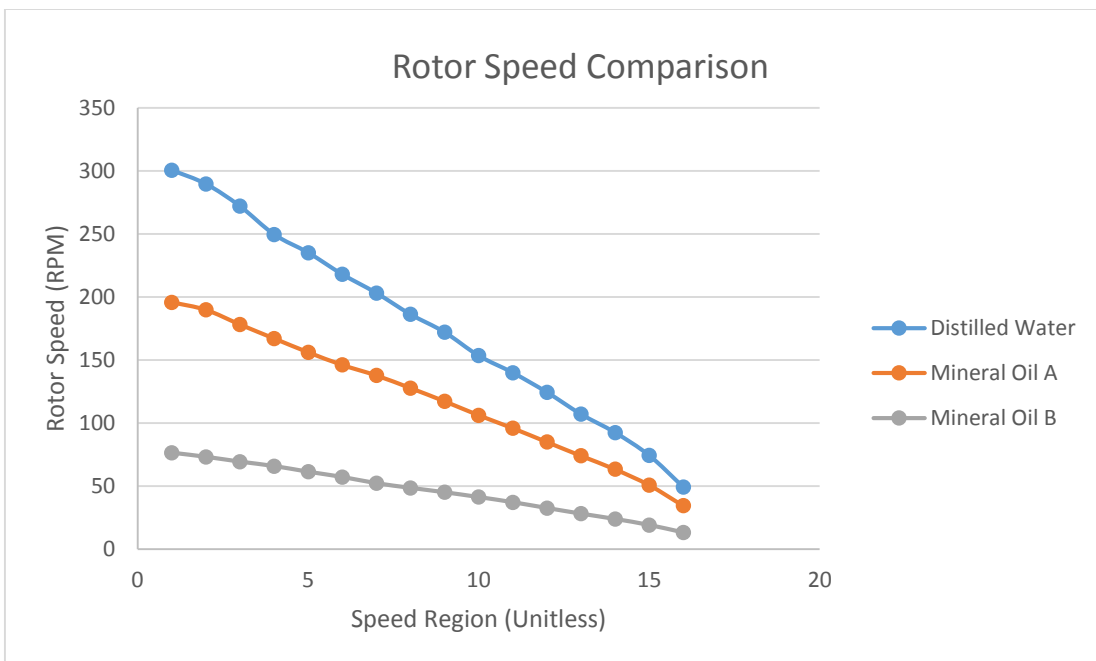


Figure H-5: Rotor speed comparison for three test fluids over specific speed regions.

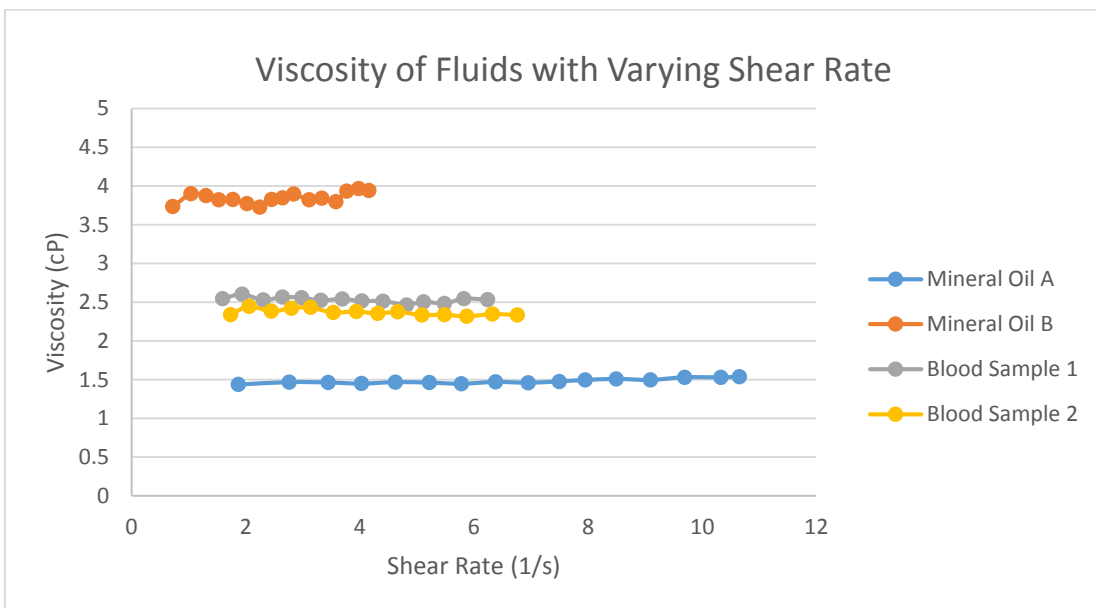


Figure H-6: Fluid Viscosity for Mineral Oil A & B and Blood at a full range of tested shear rates.

Table H-5: Tabulated Viscosity of Mineral Oil A & B

Speed Region	Distilled Water	Mineral Oil A	Mineral Oil B	Shear Rate for A	Shear Rate for B	Ratio W/A	Viscosity A	Ratio W/B	Viscosity B
1	300.5854211	195.7860526	76.39126316	10.65310919	4.156600824	1.535274944	1.538345494	3.934814122	3.94268375
2	289.63	189.7587	73.1411	10.32514893	3.979752971	1.526306831	1.529359444	3.959880286	3.967800047
3	272.0016	178.1448	69.2997	9.693213489	3.770734744	1.526856804	1.529910518	3.925004004	3.932854012
4	249.6063	167.0714	65.8296	9.090687733	3.581919689	1.494009747	1.496997766	3.791703124	3.799286531
5	235.1191	156.1234	61.3107	8.494985241	3.336037337	1.505982447	1.508994412	3.834878741	3.842548498
6	218.0071	146.0721	57.1728	7.948073983	3.110885954	1.492462284	1.495447209	3.813126172	3.820752424
7	203.1242	137.7182	52.2249	7.49352164	2.841660858	1.474926333	1.477876188	3.889412905	3.89719173
8	186.2533	127.7369333	48.5323	6.950421035	2.640739135	1.458100607	1.461016808	3.837718385	3.845393822
9	172.1008	117.2455	45.0475	6.379561245	2.451124224	1.467866997	1.470802731	3.820429547	3.828070406
10	153.4368	106.1758	41.2427	5.777236814	2.244097475	1.445120263	1.448010503	3.720338387	3.727779064
11	139.9568	95.9108	37.1525	5.218697713	2.021541545	1.45923921	1.462157688	3.767089698	3.774623877
12	124.4702	84.9264	32.5861	4.621014624	1.773074623	1.465624352	1.468555601	3.819732954	3.82737242
13	107.0903	73.9974	28.0859	4.02634596	1.528209775	1.447217064	1.450111499	3.812955967	3.820581879
14	92.4785	63.3095	23.8998	3.444796028	1.300435734	1.46073654	1.463658013	3.869425686	3.877164537
15	74.4072	50.7683	19.1227	2.762404349	1.040504205	1.465623233	1.46855448	3.891040491	3.898822572
16	49.3315	34.3954	13.2371	1.871522241	0.720256983	1.434247021	1.437115515	3.726760393	3.734213914
				Average	1.478724668	1.481682117	3.838394429	3.846071218	

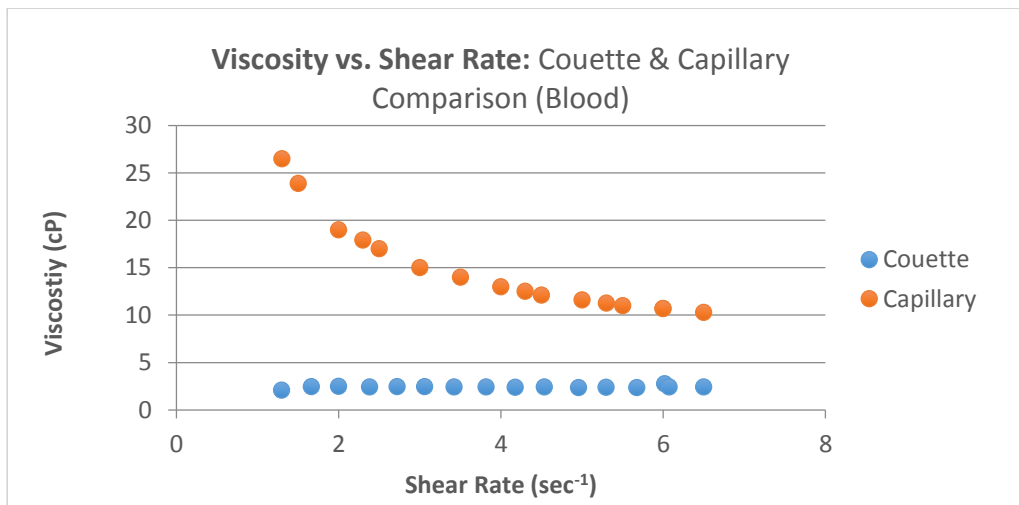


Figure H-7: Blood viscosity comparison between this couette viscometer and Dr. Cho's capillary tube system.

Hematocrit Measurement



Figure H-8: Pre-viscosity test hematocrit measurement.

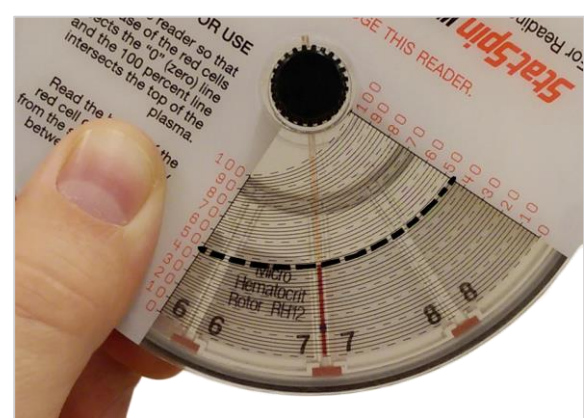


Figure H-9: Post-viscosity test hematocrit measurement.

Magnetism Measurements

Location	Avg. Field Strength (uT)
Top	1714.2
Front	1216.2
Back	695.92
Left	1088.9
Right	889.99

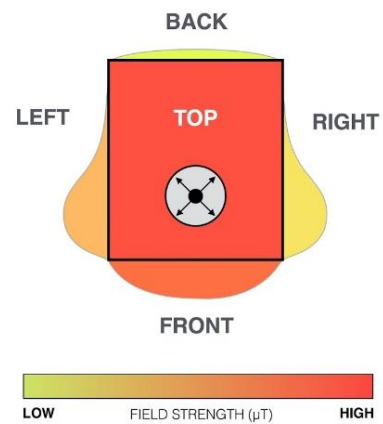


Figure H-10: Magnetic field strength data values and heat map.

Dynamic Eccentricity

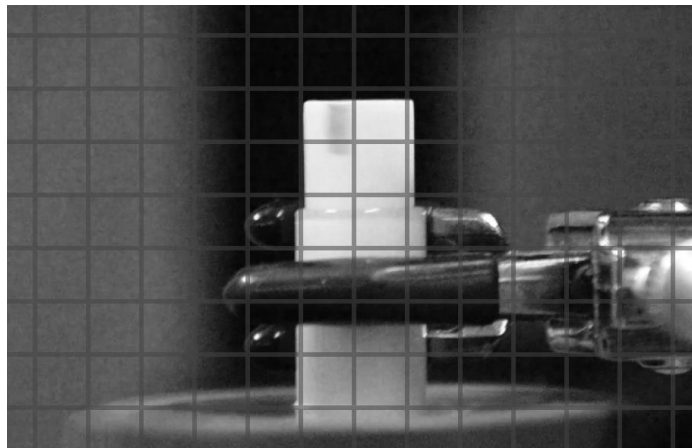
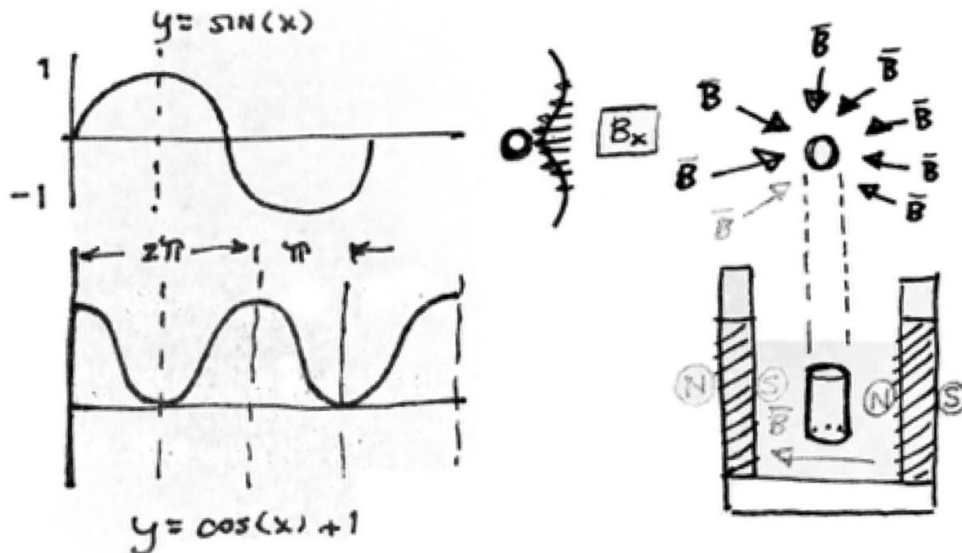


Figure H-11: Rotor wobbling analysis image.

EDDY CURRENT

ANALYSIS



ASSUMPTIONS

1. Magnetic field varies as sinusoid
2. Gap is small enough that field lines are straight across
3. Wave function estimation
4. Amplitude = maximum field strength

EQUATIONS

$$dB_x/dt = -(2\pi\omega B)\sin(2\pi\omega t)$$

*based on geometry and assumptions

$$\oint E \cdot ds = -d\Phi_B/dt$$

*Faraday's Law

GIVEN

$$B = 0.137 \text{ Tesla}$$

*field strength between 2 neodymium bar magnets 1 inch apart

$$\omega = 500 \text{ rev/min}$$

*motor rotational speed

$$T = 0.12 \text{ sec/rev}$$

*period of rotation

$$D = 0.25 \text{ inch}$$

*diameter of aluminum insert

$$h = 1.75 \text{ inch}$$

*height of aluminum insert

SOLUTION

$$E(2\pi)(D) = -(D)(h)dB_x/dt$$

$$E = (h/2\pi)(-dB/dt) = (\omega B)[\sin(2\pi\omega t)]$$

⇒ Evaluate over time to get temporal profile for electric field strength in rotor.

Appendix I: Experimental and Developmental Protocols

PR-33 Design of an Automated Couette Viscometer

Protocol: Temperature Retention Testing

Tested by: Dan Nguyen, Matthew Lorenz

1. Purpose of Test

- 1.1. Retaining the blood samples at a temperature of 37°C or 98.6 °F, body temperature, for the duration of the test is not essential, but highly preferred. In order to record viscosity, retaining the temperature is not necessary because the blood is anticoagulated; however, results will be more accurate if the test conditions are physiologically relevant.

2. Test Plan

2.1. Specifications

- 2.1.1. Blood sample to retain temperature of 37°C or 98.6 °F for the duration of the test, approximately 2 minutes. The temperature is allowed to reach 90.0 °F by the end of the test.

2.2. Pass/Fail Criteria

- 2.2.1. Pass if the temperature retained at the end of 2 minutes is below 90.0 °F.

2.3. Test Equipment

2.3.1. Aluminum Block Fixture

2.3.2. Heating System with 6" heating element and thermocouple

2.4. Test Equipment needed but not available

2.4.1. Vacutainers

2.4.2. 12-V power supply

2.5. Phases of Testing

3. Test Procedure

3.1. Setup Instructions

- 3.1.1. Safety glasses and gloves should be worn for duration of testing.

- 3.1.2. The temperature of the environment should be regulated to 68 °F or room temperature.

- 3.1.3. Plug in heating system without the heating element first.

- 3.1.4. Program the heating system using instructions given to set to 98 °F as the lower limit and 99 °F as the higher limit.

- 3.1.5. Setup the heating element into the aluminum block as shown in Figure J-1.

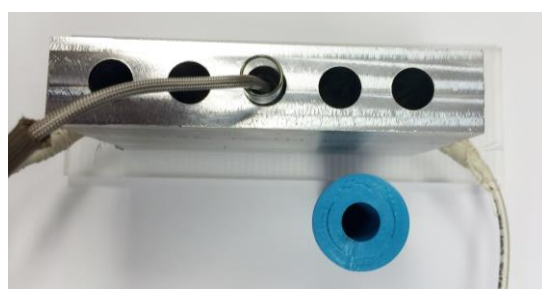


Figure I-1: Heating element and thermal retention experimental setup.

3.2. Testing Procedure

3.2.1. Plug in heating element into heating system.

3.2.1.1. **Caution: It may get very hot initially but will reach an equilibrium**

3.2.2. Place vacutainers inside the aluminum block fixture and have the thermocouple touch the inside bottom of the vacutainer that is heating. Do this for 30 minutes.

3.2.3. After the duration of 30 minutes, remove the vacutainer with the thermocouple still touching the inside bottom of the vacutainer and start the 2 minute timer. When removed, the temperature should initially be between the range set.

3.2.4. Record the temperature using the thermocouple after the 2 minute duration.

3.2.5. Perform steps 3.2.2-3.2.4 with a sample size of 10.

4. Test Results

4.1. Core Results

Initial Temperature (°F)	Final Temperature (°F)
97	90
97	90
98	91
100	92
100	92
101	92
102	93
102	93
102	93

4.2. Pass/Fail

4.2.1. According to the Pass/Fail criteria, these trials have passed.

5. Design Summary

5.1. The temperature retainment is affected by various factors. The most important factors are the heating environment and the material of the vacutainer. There was a limit onto the material of the vacutainer since most are made out of glass. The heating environment was a factor that could be more controlled. Using the aluminum block fixture had shown greater success to retaining the temperature through duration of 2 minutes. Further experimentation and testing will involve discovering a better environment.

PR-33 Design of an Automated Couette Viscometer

Motor Test Setup Procedure

Tested by: Dan Nguyen, Austin Farber

6. Purpose of Test Setup Procedure

6.1. This test procedure will allow the technician to follow instructions to properly test their sample.

If the technician needs to change the program, these instructions will present how to safely do that as well.

7. Test Setup Procedure

7.1. Setup Instructions

7.1.1. Gloves should be worn for duration of testing and setup to guarantee no potential for shock.

7.1.2. Connect the power source to the bread board, with positive (red) on a different row than the negative (black) as shown in Figure 1.

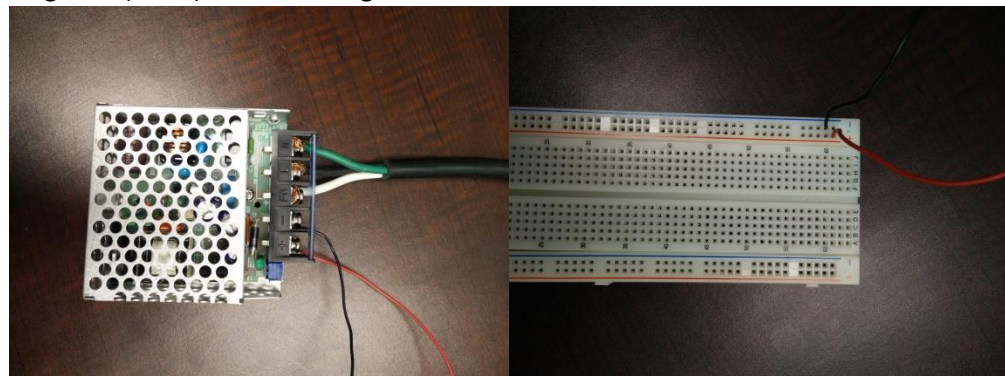


Figure I-2: Connection between Power Source and Breadboard

7.1.3. Create a bridge across the bread board. Connect the motor to the controller via fitted cap.

Connect the controller to the correct column. For example, in Figure 2, the negative is connected to the left side of the column across the bridge. In that same column, that is where the negative side of the controller should be placed.

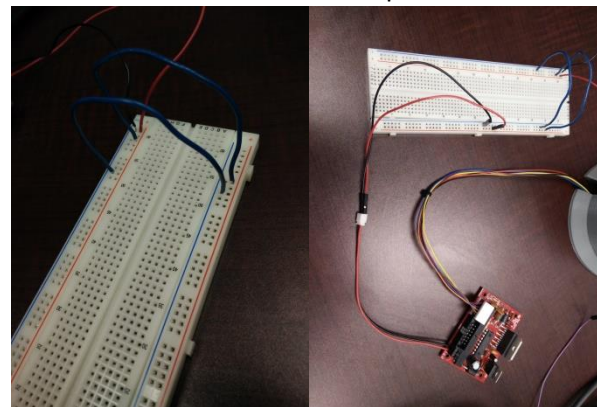


Figure I-3: Bridging across the Bread Board and Connecting the Motor

7.1.4. Connect the AC/DC converter to the bread board as shown in Figure 3. The top wire (green) is the positive while the bottom wire (blue) is the negative. Align it with the correct column similar to the motor.

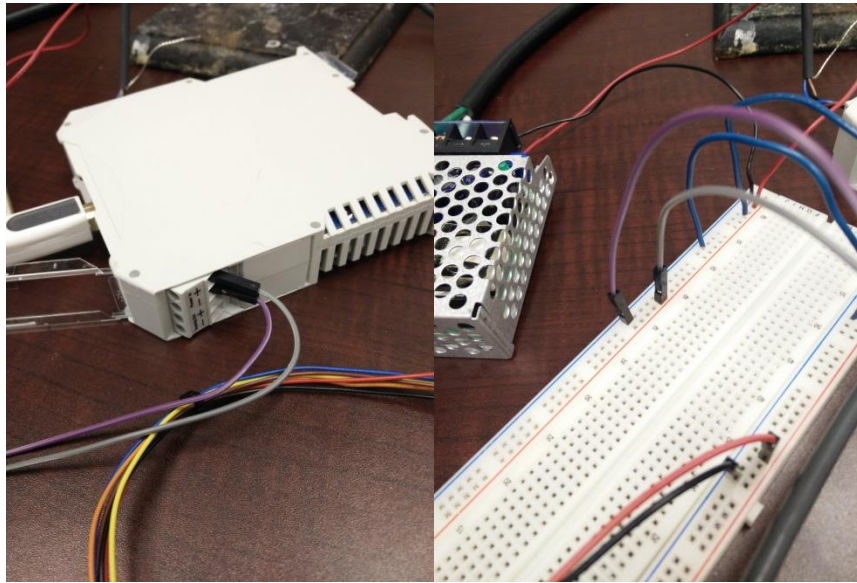


Figure I-4: Connecting AC/DC converter to Bread Board

7.1.5. Connect the AC/DC converter to the computer via USB as shown in Figure 4. Type B USB wire needed. Once the tachometer is positioned, connect the power supply to a 12-V outlet for the motor to turn on and the run the program.



Figure I-5: Connecting AC/DC Converter to Computer via USB

8. Programming Setup Procedure

- 8.1. In case a change in the program is desired to be altered, start out by removing the bridge in the bread board from the power supply to the controller.



Figure I-6: Remove bridge from Power Supply to Controller

- 8.2. Connect the programmer to the controller using the connector and to the computer via USB.

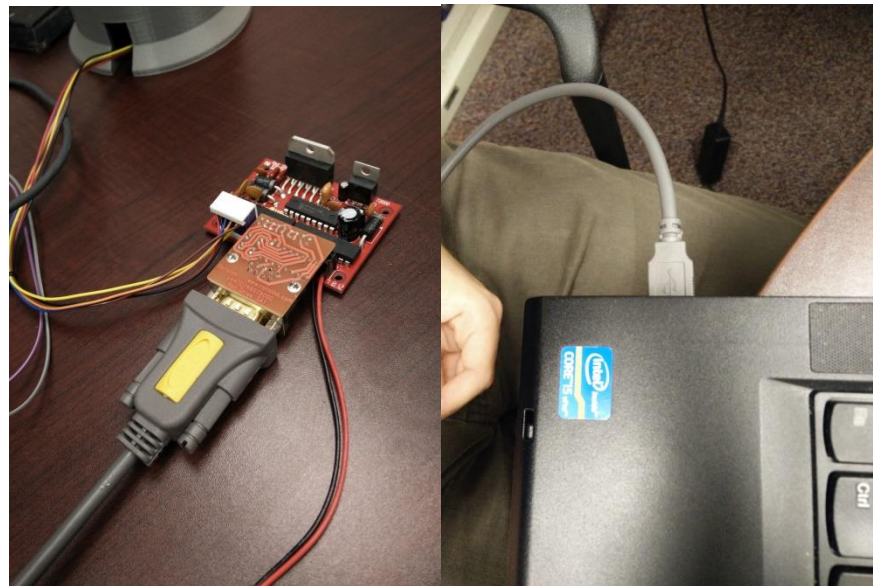


Figure I-7: Connect Programmer to Controllers and Computer

8.3. Once the program is successfully downloaded to the control, the bridge can be connected again. Connect the power supply to the 12-V outlet for the motor to turn on and run the new desired program.

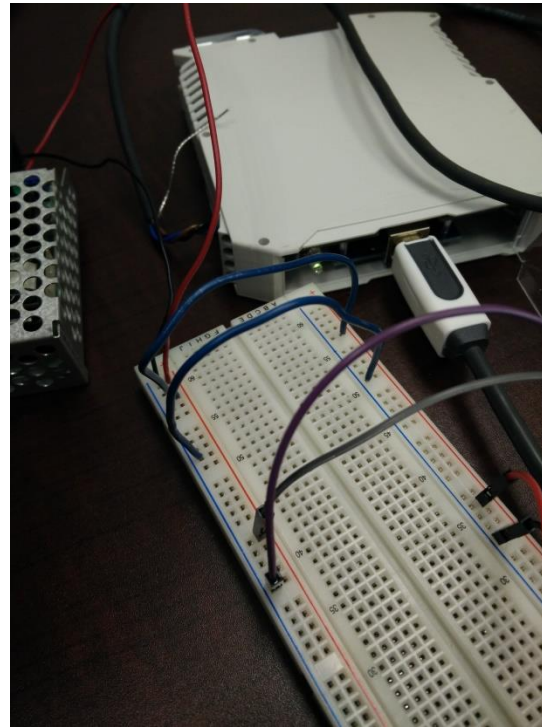


Figure I-9: Reattach the Bridge from the Power Supply to Controller

Appendix J: Bill of Materials

Seller	Manufacturer	Product Name	Product ID (If Applicable)	Quantity	Cost	Reason for Purchase
Monarch Instrument	Monarch Instrument	ROS-L-V (Laser Sensor)	6180-030	1	196	Laser Sensor for Tachometer
Monarch Instrument	Monarch Instrument	F2A3X (Frequency to Analog Converter)	F2A3X	1	239	Converter to read data in real-time for Tachometer
Rotalink	Rotalink	D2431-09451	D2431-09451	1	-	Motor system to be used to control testing
Rotalink	Rotalink	DC1A	DC1A	1	-	Control board for interfacing with the motor
Rotalink	Rotalink	Encoder	N/A	1	237.81	Encoder used to measure shaft speed
Rotalink	Rotalink	Gear Box Type 210	N/A	1	-	Gear box needed to lower high rpm to low rpm
Rotalink	Rotalink	Red Link CD Software	N/A	1	-	Software for programming the control board
Digikeg	TDK-Lambda Americas Inc	285-1253-ND	HK 15A - 121A	1	42.42	Not Purchased but needed for Product AC to DC power supply
Lowe's Home Center, LLC	Utilitech	18562 UUTL 10-FT T4-GAUGE REPLC	18562	1	14.81	Power cable for AC to DC conversion
Sparkfun	Sparkfun	Machine Screw - Socket Head (6-32, 1/2", 25 pack)	ROB-12415	25	2.19	Attach magnet housing to motor shaft
McMaster-Carr	McMaster-Carr	2" Long x 0.25" Wide x 0.25" Thick (Neodymium Nickel-Plated)	5849K76	1	22.59	Test strength of magnet and feasibility of eddy current method.
McMaster-Carr	McMaster-Carr	Chemical-Resistant (Type I) PVC Rod 2" OD x 1' Long	8745K26	2	22.4	Construction of rotating magnet assembly.
McMaster-Carr	McMaster-Carr	2" Long x 0.25" Wide x 0.25" Thick (Neodymium Nickel-Plated)	5849K76	1	26.32	(Replacement) Construction of rotating magnet assembly.
McMaster-Carr	McMaster-Carr	Chemical-Resistant (Type I) PVC Rod 2" OD x 1' Long	5739K78	2	3.46	Construction of rotating magnet assembly.
Amazon	UFIBEST®	6.8" RS232 DB9 9-Pin Female to USB 2.0 PL2303 Serial Cable	B000NVJW8VE	1	3.39	Serial connection cable from motor controller to PC (shipping cost).
Amazon	UGREEN	6' RS232 DB9 9-Pin Male to USB 2.0 PL2303 Serial Cable	B000UZ2Y4V0	1	3.39	Serial connection cable from motor controller to PC.
McMaster-Carr	McMaster-Carr	1.25" Long x 0.25" Wide x 0.25" Thick (Ceramic High-Temp)	5739K78	2	11.29	Construction of rotating magnet assembly.
Amazon	Amazon	7075 Aluminum Rod (0.675" OD x 24" Long)	B000H9NWK2	1	21.44	Rotor construction material.
McMaster-Carr	McMaster-Carr	6061 Aluminum Tube, 0.250" OD x 0.180" ID (0.035" Wall X 2' Long)	9056K61	1	19.99	Rotor construction material.
Rotalink	Rotalink	D2431-09451	D3650-3540	1	152.37	Motor system to be used to control testing.
COMAD Westphal	Hybrid Lab	Rotor Rapid Prototype (Objet)	N/A	6	25.36	Rotor construction material.
Amazon	Adventurer's Bag	TDK Lambda Power Supply (10V, 12V, 900mA)	B00FH3A4BV2	1	64.28	Power Supply replacement.
Amazon	Direct Care Store	13x75 (4.5ml) BD Blood Collection Vacutainer [Model #369714]	B0015T97K4	1	35.19	Vacutainers for measurement and analysis.
McMaster-Carr	McMaster-Carr	2" Long x 0.25" Wide x 0.25" Thick (Neodymium Nickel-Plated)	5849K76	3	63.11	Magnets Rotation (Validation Tool)
COMAD Westphal	Hybrid Lab	Rotor Rapid Prototype (Objet)	N/A	4	16.45	Rotor construction material.
COMAD Westphal	Hybrid Lab	Motor Enclosure (Cubex)	N/A	1	10	Motor enclosure material.
Sparkfun	Sparkfun	Screw Set Metric 1/4"-20 x 1/2"	ROB-12488	2	13.39	Attach magnet housing to motor shaft.
BriskHeat	BriskHeat	SDC 120V J-TYPE DEG F 120 VAC J	SDC120JF-A	1	215.2	Materials for temperature control.
BriskHeat	BriskHeat	FIBROX HTG CORD 6'	HTC450007	1	43.2	Materials for temperature control.
COMAD Westphal	Hybrid Lab	Rotor Rapid Prototype (Objet)	N/A	4	23.8	Heating container construction.
Plaza Art Supplies	Elmer's	Elmer's Wood Glue	402100	1	2.91	Housing
Plaza Art Supplies	Plaza Art Supplies	Bass wood 1/8" x 8 x 24	483161	1	7.29	Housing
Plaza Art Supplies	Plaza Art Supplies	Craft Plywood 1/8" x 12 x 24	483485	1	4.49	Housing
McMaster-Carr	McMaster-Carr	Multipurpose 6061 Aluminum, Rectangular Bar, 1" X 3", 1/2" Long	8975K239	1	23.79	Heating container construction.
McMaster-Carr	McMaster-Carr	Multipurpose 6061 Aluminum Rod, 1/4" Diameter, 1/2" Long	8974K22	1	4.17	Heating container construction
McMaster-Carr	McMaster-Carr	Multipurpose 6061 Aluminum, Rectangular Bar, 1/2" X 1", 1/2" Long	8975K11	1	5.9	Heating container construction
			Total:		\$1,645.20	

Appendix K: Final Gantt Chart

